

1 **Revised version 1**

2 **Dissolution mechanisms of chromitite:**

3 **Understanding the release and fate of chromium in the environment**

4  
5 Michael Schindler<sup>1\*</sup>, Aaron J. Lussier<sup>1,3</sup>, Emilia Principe<sup>1,2</sup>, and Nadia Mykytczuk<sup>2</sup>

6 1. Department of Earth Sciences, Laurentian University, Sudbury, ON, Canada, P3E 2C6

7 2. School of the Environment, Laurentian University, Sudbury, ON, Canada, P3E, 2C6

8 3. Canadian Museum of Nature, P.O. Box 3443, Station D, Ottawa, ON, Canada, K1P 6P4  
9

10  
11  
12  
13  
14  
15  
16  
17  
18  
19  
20  
21  
22  
23  
24  
25 \*corresponding author: [mschindler@laurentian.ca](mailto:mschindler@laurentian.ca)  
26

27 **ABSTRACT**

28 An understanding of the formation of toxic hexavalent chromium ( $\text{Cr}^{6+}$ ) in Cr-containing  
29 mine tailings and associated soils and sediments, requires an understanding of the underlying  
30 dissolution mechanisms of chromitite, a common chromite-bearing rock in both ophiolites suites  
31 and ultramafic intrusions. This study will examine dissolution mechanisms of chromitite in  
32 various acidic, neutral and alkaline solutions containing cultivated bacteria, manganese oxides,  
33 sulfates and phosphates. Dissolution of chromitite is non-stoichiometric under acidic, near-  
34 neutral and alkaline pH conditions and involves the release of chromite nanoparticles and  
35 complex dissolution/re-precipitation reactions. Chromitite samples are obtained from the Black  
36 Thor chromite deposit in Northern Ontario, Canada; part of the 'Ring of Fire' intrusive complex.  
37 The examined chromitite is composed of chromite,  $(\text{Fe}_{0.5}\text{Mg}_{0.5})(\text{Al}_{0.6}\text{Cr}_{1.4})\text{O}_4$  and clinochlore;  
38  $\text{Mg}_3[\text{Si}_4\text{O}_{10}(\text{OH})_2] \times (\text{MgAl}_{1.33}(\text{OH})_6)$ , the latter phase contains ~3 wt% Cr in the form of chromite  
39 nanoparticles. Bulk dissolution data are collected after dissolution experiments with chromitite  
40 powders, and the chemical and mineralogical composition of treated chromitite surfaces is  
41 characterized with a combination of surface analytical techniques (X-ray photoelectron  
42 spectroscopy) and nano- to micro-analytical techniques (scanning electron microscopy,  
43 transmission electron microscopy and focused ion beam technology). In the chromitite systems  
44 studied here, the non-stoichiometric dissolution of clinochlore is the dominant reaction, which  
45 results in the formation of a hydrous and porous silica precipitate that is depleted in chromite  
46 nanoparticles relative to untreated clinochlore. Complete replacement of clinochlore by hydrous  
47 silica on the surface of chromitite under acidic conditions promotes the release of chromite  
48 nanoparticles and results in higher Cr:Si in solutions and in higher proportions of secondary Cr  
49 species on its surface (secondary Cr species are defined as surface terminations that do not  
50 occur on an untreated chromite surface, such as  $-\text{Cr}^{3+}-\text{OH}_2$  and  $-\text{Cr}^{6+}-\text{OH}$ ). Cultivated bacteria  
51 from a sulfide-bearing acid-mine drainage system affect neither the degree of dissolution nor the  
52 formation of secondary Cr species, whereas pyrolusite ( $\text{MnO}_2$ ) particles, and adsorbed or

53 precipitated Fe- and Al-bearing hydroxide, -sulfate and -phosphate species, affect release and  
54 re-adsorption of chromite nanoparticles and Cr-bearing species during dissolution of chromitite  
55 under acidic, neutral and alkaline conditions. These results show that weathering of chromitite  
56 and the release of Cr into the environment are strongly controlled by factors such as dissolution  
57 rates of Cr-bearing silicates and chromite, the release of chromite nanoparticles, re-precipitation  
58 of amorphous silica, the presence of particles in solution and the pH-dependence adsorption (or  
59 precipitation) of Fe- and Al-bearing hydroxides and sulfates.

60 Keywords: chromite, clinochlore, dissolution, chromate, toxicity, Ring of Fire, X-ray  
61 photoelectron spectroscopy, transmission electron microscopy, focused ion beam, bacteria,  
62 pyrolusite

63

## 64 INTRODUCTION

65 Effectively assessing the environmental risks posed by highly toxic hexavalent chromium  
66 ( $\text{Cr}^{6+}$ ) in Cr-containing mine tailings, as well as associated soils and sediments, requires an  
67 understanding of (1) its occurrence and speciation in minerals and glasses (i.e., slags), (2) the  
68 solubility and dissolution behaviour of such phases, (3) the complex redox chemistry of released  
69 Cr species, (4) the chemical reactions that influence the mobility of Cr species in soils and  
70 sediments; and (5) the occurrence and behavior of nano-scale chromite particles.

71 In a recent study at the nanoscale, Schindler et al. (2017) showed that chromite  
72 nanoparticles are held within clinochlore and lizardite grains in chromitite ore from the Black  
73 Thor chromium deposit in Northern Ontario, Canada and the Mistake mine, part of the  
74 Franciscan Ophiolitic Complex. This is an important observation as the potential release of  
75 chromite nanoparticles rather than  $\text{Cr}^{3+}$  aqueous species during the weathering of chromite-  
76 bearing silicate minerals will have an impact on the environmental behavior of  $\text{Cr}^{3+}$  and its  
77 potential oxidation to  $\text{Cr}^{6+}$ . The study by Schindler et al. (2017) did not address the dissolution of  
78 the larger chromite grains or the roles of bacteria, manganese oxide particles and mineral

79 surface coatings during dissolution and release of the Cr-rich silicates and chromite  
80 nanoparticles, respectively. This study will further investigate the dissolution mechanisms of  
81 chromitite from the Black Thor chromium deposit focusing on chemical reactions on surfaces of  
82 millimeter-size slabs and the geochemical behavior of released elements and chromite  
83 nanoparticles during the dissolution reactions.

84 Chromitite is an ultramafic rock composed predominantly of the spinel group mineral  
85 chromite ( $\text{FeCr}_2\text{O}_4$ ) with minor silicates phases (e.g., serpentine, chlorite, amphibole, pyroxene  
86 and olivine groups). It is a common rock in both ophiolite suites and ultramafic intrusions, the  
87 latter being exemplified by the Bushveld Igneous Complex in South Africa, the Stillwater  
88 Igneous complex in Montana, and the current region of interest. Larger rock fragments, grains,  
89 and particulate matter derived from chromitites may occur in soils and tailings piles in close  
90 proximity to natural outcrops or mining activities, respectively (Pillay et al. 2003; Oze et al. 2004;  
91 Tiway et al. 2005; Kien et al. 2010). Although the total amount of Cr in chromitite may be  
92 controlled by the abundance of refractory chromite, the bioavailability of Cr and formation of  
93 hexavalent Cr may ultimately depend on the weathering of serpentine and chlorite group  
94 silicates, as they have been shown to be more susceptible to weathering (e.g., Oze et al. 2004,  
95 2007; Fandeur et al. 2009; Hseu and Iizuka 2013; Morrison et al. 2015). For instance, elevated  
96  $\text{Cr}^{6+}$  concentrations in soil pore water and groundwater have been reported for serpentinite-  
97 bearing soils and aquifers (e.g., Izbicki et al. 2008; Wood et al. 2010). On the contrary,  
98 spectroscopic studies on the speciation of Cr in serpentine-derived soils from other locations  
99 indicated the absence of detectable amounts of  $\text{Cr}^{6+}$  (Hseu and Iizuka 2013; Fandeur et al.  
100 2009), and hence many aspects of this issue remain unresolved.

101 Understanding the redox chemistry of Cr is a critical aspect of determining its toxicity. As  
102 a trivalent cation, chromium has relatively low toxicity, is a micronutrient, and is relatively  
103 insoluble and immobile at neutral to alkaline pH. In contrast, hexavalent chromium is a  
104 significant environmental toxicant, a human carcinogen, and is highly mobile at neutral-to-

105 alkaline pH (e.g., Fendorf 1995). The complexity of  $\text{Cr}^{3+}/\text{Cr}^{6+}$  redox reactions in natural and  
106 anthropogenic systems can make effective risk assessment difficult. For example,  $\text{Cr}^{3+}$  can be  
107 readily oxidized to  $\text{Cr}^{6+}$  by naturally occurring  $\text{Mn}^{3+}/\text{Mn}^{4+}$ -oxides (Bartlett and James 1979; Eary  
108 and Rai 1987; Fendorf 1995; Weaver and Hochella 2003; Oze et al. 2007), whereas  $\text{Cr}^{6+}$  can be  
109 reduced to  $\text{Cr}^{3+}$  by organic carbon, bacteria (aerobic and anaerobic conditions), sulfides and  
110  $\text{Fe}^{2+}$ -bearing species and clay minerals (e.g., Kamaludeen et al. 2003; Parrhasarathy et al.  
111 2003). Hence, understanding the dissolution mechanisms of chromitite under different pH  
112 environments and in the presence of manganese oxides and/or bacterial organisms is critical for  
113 assessing aspects of the health risks associated with chromitite-rich rocks, soils and tailings.

114 The dissolution mechanisms of chromitite in the presence of different types of acids,  
115 bases, and oxidants at varying temperatures have been thoroughly studied to improve the  
116 leaching efficiency of Cr from the ore at temperatures commonly above  $100^{\circ}\text{C}$  (e.g., Zhang et  
117 al. 2016). A common process involves the dissolution of chromitite in oxidizing alkaline solutions  
118 which results in the formation of water-soluble chromate species, allowing the physical  
119 separation of Cr from the silicate minerals. Less soluble chromate phases, such as the  
120 carcinogenic calcium chromate ( $\text{CaCrO}_4$ ), remain with the silicate residue and require special  
121 treatment or waste disposal. An alternative extraction process is the treatment of chromitite with  
122 sulfuric acid, which results in the formation of amorphous silica on the surface of the chromitite  
123 and in the simultaneous release of Cr, Al, Fe and Mg into solution (Zhao et al. 2014). This  
124 process requires the separation of the latter elements, which can be achieved via the  
125 precipitation of Fe-hydroxides at higher pH in the presence of an oxidant such as  $\text{H}_2\text{O}_2$  (Zhang  
126 et al. 2016).

127

## 128 **Detailed objectives and approach**

129 The observation that Cr occurs in the form of chromite nanoparticles in silicate minerals  
130 within high-grade chromitite ore from the Black Thor chromite deposit requires a unique multi-

131 analytical approach to characterize the dissolution mechanisms of the ore at ambient Earth  
132 surface temperatures. As such, this study will combine transmission electron microscopy with  
133 surface sensitive methods such as X-ray photoelectron spectroscopy, and bulk dissolution data  
134 to examine release, dissolution, re-adsorption and attachment of chromite nanoparticles and Cr-  
135 bearing aqueous species during chromitite dissolution experiments. The occurrence of chromite  
136 nanoparticles in solution and their proportion relative to Cr-bearing solutes will be addressed  
137 elsewhere.

138 This study will aim specifically to examine whether:

- 139 (a) the minerals in the ore samples dissolve stoichiometrically or non-stoichiometrically  
140 under conditions that may occur in potential mine waste environments;
- 141 (b) the amphoteric elements Al, Fe, and Cr behave similarly during dissolution in acidic,  
142 neutral, and alkaline conditions;
- 143 (c) the chemical composition of solutions after the experiments can be directly linked to the  
144 composition of altered ore mineral surfaces and *vice versa*;
- 145 (d) any secondary Cr species (i.e., those not found on untreated chromitite, such as  
146 hydrated  $\text{Cr}^{3+}$  and  $\text{Cr}^{6+}$  species) occur on treated chromitite surfaces;
- 147 (e) bacteria from oxidized portions of sulfide-rich mine tailings affect the dissolution of  
148 chromitite under aerobic acidic conditions and contain populations that grow  
149 preferentially in Cr-bearing media;
- 150 (f)  $\text{MnO}_2$  particles affect the dissolution of chromitite and specifically the proportion of  
151 hexavalent Cr species, on both  $\text{MnO}_2$  and altered chromitite surfaces;
- 152 (g) potential liming of tailings material through the addition of e.g.,  $\text{CaCO}_3$  affects the  
153 dissolution mechanisms and the proportion of  $\text{Cr}^{6+}$  species on altered chromitite  
154 surfaces.

155 In typical studies of mineral dissolution, powders of known total surface area are used,  
156 and the chemical reactions are deduced by subsequent bulk compositional analyses of

157 solution and solid phase materials. Here, two types of experiments are conducted: (1)  
158 utilizing powdered chromitite materials, and (2) using single slabs, manually cut from  
159 chromitite rock pieces. Powder-based experiments result in the release of sufficient amounts  
160 of ions to solution during the dissolution process, thereby facilitating quantification by  
161 standard solution chemical analytical techniques. However, the relatively flat surfaces of the  
162 slabs are better-suited for studying the chemical reactions occurring on mineral surfaces, as  
163 similar locations on their surfaces can be examined with a multi-analytical approach,  
164 integrating data from X-ray photoelectron spectroscopy (XPS), scanning electron  
165 microscopy (SEM), *in situ* focused ion beam (FIB) sample extraction, and transmission  
166 electron microscopy (TEM) techniques. Noteworthy disadvantages of working with chromitite  
167 slabs, however, are that their surface composition, area, and roughness cannot be faithfully  
168 reproduced between individual experiments, and the very low quantities of ions released  
169 into solution are often below the detection limits of even the most sensitive analytical  
170 methods. Hence, with material extraction from the same chromite sample, concurrent  
171 dissolution experiments are run, one utilizing chromitite slabs and the other utilizing  
172 chromitite powders. Comparing the results from both approaches allows greater  
173 understanding of the overall, underlying dissolution mechanisms of chromitite ore.

174

## 175 **METHODS**

176 A high grade chromitite ore sample was obtained from the Black Thor chromite deposit,  
177 Ontario, Canada, through the Ontario Geological Survey. The Black Thor chromite deposit is  
178 part of the Neoproterozoic 'Ring of Fire' Intrusive Complex, located in the Oxford-Stull Domain of  
179 the Archean Superior Province, and interpreted as an intercratonic rift basin separating the  
180 Mesoproterozoic North Caribou and Hudson Bay Terranes (Stott et al. 2010). Cumulate chromite  
181 occurs throughout much of the deposit and occurs as a continuous, thickly-bedded chromitite  
182 horizon at the transition from olivine-dominant to pyroxene-dominant lithologies (Weston and

183 Shinkle 2013; Laarman 2013).

184

### 185 **Sample preparation**

186 Both powders and slabs were prepared from the same chromitite sample. Chromitite slabs  
187 with dimensions of circa 5 x 5 x 3 mm<sup>3</sup> were prepared with a petrographic micro saw. Powders  
188 (100 mg for each experiment) were prepared by crushing and milling the remaining rock sample  
189 to an average grain size of 75 ±10 µm (determined by optical microscopy). All samples were  
190 thoroughly washed with double-deionized water prior to initial analyses by optical microscopy,  
191 SEM, XPS, TEM, X-ray diffraction (XRD), and X-ray fluorescence spectroscopy (XRF).  
192 Experiments and analytics are carried out for chromitite slabs in the sequence (1) dissolution  
193 experiment, (2) XPS, (3) SEM, (4) TEM and for powders in the sequence (1) dissolution  
194 experiment, (2) ICP-OES (solution), (3) XPS (selected samples).

### 195 **Dissolution experiments with and without MnO<sub>2</sub> particles and bacteria**

196 Dissolution experiments were carried out on chromitite slabs and powders for four weeks  
197 at the pH-values and chemical compositions listed in Tables 1-2 and A1-A3. Both initial and final  
198 pH and Eh values were determined using a standard hydrogen electrode calibrated against pH  
199 solutions of pH 4, 7 and 10 and a K-iodide standard. The standard deviation of individual  
200 measurement pH and Eh measurements is circa ± 0.2 units, based on repeated measurements  
201 of the standard solutions.

202 Manganese oxide phases containing Mn<sup>3+</sup> (e.g., birnessite, (Na,Ca)<sub>0.5</sub>(Mn<sup>4+</sup>, Mn<sup>3+</sup>)<sub>2</sub>O<sub>4</sub>  
203 (H<sub>2</sub>O)<sub>1.5</sub> are commonly more reactive and stronger oxidants of Cr<sup>3+</sup> than those containing  
204 exclusively Mn<sup>4+</sup> (e.g., pyrolusite, MnO<sub>2</sub>) (Weaver and Hochella 2003). Manganese (III)-bearing  
205 oxides are more common in soils, whereas Mn<sup>4+</sup>-bearing oxides such as pyrolusite occur  
206 predominantly in coal fly ashes and smelter waste products formed at higher *T* (Eary and Rai  
207 1987). To better assess the alteration of chromitite in mine and smelter wastes, dissolution

208 experiments were thus conducted with pyrolusite powder (US Research Nanomaterials,  
209 average grain size 7.98  $\mu\text{m}$ ) under acidic, neutral and alkaline pH conditions (Tables 1-2).  
210 Solutions during the dissolution experiments were not protected from solar radiation as Weaver  
211 and Hochella (2003) showed that this had no effect on the oxidation of  $\text{Cr}^{3+}$  aqueous in the  
212 presence of pyrolustite.

213 Bacteria sensitive or resistant to  $\text{Cr}^{6+}$  can reduce the ion to  $\text{Cr}^{3+}$  under aerobic and  
214 anaerobic conditions, even if they have not been exposed to high concentrations of Cr in the  
215 past (e.g., Kamaludeen et al. 2003). At the Black Thor chromite deposit, chromitite is over- and  
216 underlain by lithologies containing minor amounts of sulfides (pyrhotite, pyrite, chalcopyrite;  
217 Laarman 2013). Hence, small proportions of the ore may become exposed to a sulfide-rich  
218 environment in mine tailings. As such, dissolution experiments are carried out with bacterial  
219 cultures, enriched from oxidized portions of sulfide-rich mine tailings in the Sudbury area  
220 (Ontario, Canada). The growth of these cultures was completed in TK media (Tuovinen and  
221 Kelly 1974) comprised of stock solutions A and B. Solution A contains 0.51  $\text{gL}^{-1}$   $(\text{NH}_4)_2(\text{SO}_4)$ ,  
222  $\text{Mg}(\text{SO}_4)(\text{H}_2\text{O})_7$  and  $\text{K}_2\text{HPO}_4$  and is adjusted with  $\text{H}_2\text{SO}_4$  to a pH of 2.5. Solution B contains 33.5  
223  $\text{gL}^{-1}$   $\text{FeSO}_4(\text{H}_2\text{O})_7$  and is adjusted with  $\text{H}_2\text{SO}_4$  to a pH of 2.1 and mixed with solution A in a ratio  
224 of 4:1 in the final TK media. Dissolution experiments under acidic conditions but without bacteria  
225 were also carried out with the solutions A and B (using aseptic techniques) as this allowed a  
226 better evaluation of the effect of bacteria on the dissolution of chromitite under acidic conditions.  
227 Dissolution experiments simulating potential liming of chromitite-bearing mine tailings were  
228 conducted with  $\text{CaCO}_3$  powders in the presence and absence of pyrolusite particles.

229 The ionic strengths and degrees of undersaturation with respect to chromite in these  
230 solutions were calculated with the software Visual MINTEQ 2.53 (Gustafsson 2012; Table A1).  
231 The change in the microbial community during dissolution of a chromitite slab was analysed with  
232 a microbial community profile (supplementary data B1).

233

## 234 **X-ray Photoelectron Spectroscopy (XPS)**

235 The near-surface composition of treated chromitite slabs and pyrolusite powder was  
236 analyzed with a Kratos Axis Ultra X-ray photoelectron spectrometer (XPS) equipped with a  
237 magnetic-confinement charge-compensation system. The advantages of this system for  
238 insulators have been described in detail by Schindler et al. (2009a, b). A total of 10 high  
239 resolution scans were collected for the Cr 2p photoelectrons using monochromatic Al K $\alpha$   
240 radiation (1486.6 eV) and the charge-compensation system. Additionally, two survey spectra (0-  
241 1100 eV) and three high-resolution scans were collected for the Mg 1s, C 1s, O 1s, Al 2p, Si 2p,  
242 Mn 2p and Si 2p photoelectrons. High resolution scans were recorded with a step size of 0.1 eV  
243 while survey spectra were collected with a step size of 0.5 eV. For all measurements, the  
244 analyzer pass energy was 20 eV and the lens and aperture were in hybrid and slot mode,  
245 respectively, which allowed the collection of photoelectrons from an area of circa 700 x 300  $\mu$ m.

246 The electrostatic sample charging (which was not completely compensated by the  
247 charge neutralizer) was corrected by setting the binding energy of the C 1s electrons of  
248 adventitious C species on the sample surface equal to 285 eV (Wagner et al. 1979). In some  
249 cases, the binding energy of the C 1s photoelectrons can vary with the type of substrate and  
250 thus result in false shifts when referenced to other spectra. Hence, corrections applied to the Cr  
251 2p spectrum were also applied to the Mg 1s spectrum, which varies over a smaller range in  
252 binding energy for oxide and silicate surfaces (103-104 eV) than the Cr 2p peak (NIST database  
253 2012). This procedure provided more confidence in the shift applied to Cr 2p spectra and is thus  
254 crucial in terms of the determination of potential hexavalent Cr species on treated surfaces of  
255 chromitite. A detailed summary of characteristic features in the Cr 2p spectrum and their  
256 relationship to structural components on the surface of chromite are given in supplementary  
257 data B2.

258 The inelastic mean free path (IMFP) of the Cr 2p electrons is calculated to be circa 1.3  
259 nm, using the NIST XPS database (2012), the binding energy of the Cr 2p electrons (577 eV)

260 and an average specific weight of  $4.8 \text{ g cm}^{-3}$  for a chromite surface layer. Information on the  
261 chemical composition of a surface can be gained to a depth three times of the IMFP ( $3 \times 1.3 =$   
262  $3.9 \text{ nm}$ , so called information depth) (Hochella 1988).

263 Both high-resolution and survey scans were processed and quantified using the Vision  
264 2.2.6 software package. Peak fitting of the Cr 2p, Mg 1s, and C 1s was done using multiple  
265 bands with constant full width at half maximum values (FWHM). The FWHM values used in the  
266 fitting procedure were 1.2, 1.5 and 1.4 eV for the Cr 2p, Mg 1s and C 1s spectra, respectively.  
267 Bands were only included in the fitting process if inflections points, shoulders or peaks indicate  
268 the occurrence of multiplet splitting, variations in the chemical environment or changes in the  
269 valence.

270 At least two sets of spectra were taken from each mineral surface (Table 1), whereby a  
271 set of spectra includes high-resolution spectra of all major elements, C 1s and a survey scan.  
272 Using the optical imaging camera of the XPS system, the two sets of spectra were taken from  
273 areas with a higher and lower proportion of clinocllore. Proportions of Mg, Al, Si, Mn, Cr, and Si  
274 are based on high resolution scans and were calculated without considerations of the  
275 proportions of C, O, S and P on the surface (Table 1, A2). As experiments under acidic  
276 conditions were carried out in phosphate-bearing sulfuric acid solutions (Tables 1-2 and A1-A3),  
277 elemental ratios between Fe and (S + P) were also determined using the Fe 2p, S 2p and P 2p  
278 peaks in the survey scans.

279 Table 1 lists selected elemental ratios of an untreated surface and treated surfaces  
280 analyzed with multiple sets of XPS spectra and the number of recorded sets ( $N \text{ XPS}$ ). The  
281 standard deviation of a ratio between the atomic proportions of two elements is circa  $\pm 0.1$  and is  
282 based mainly on the uncertainty of the size of the quantification area in a spectrum. Table A2  
283 lists the normalized atomic proportions of Cr, Mg, Si, Al and Fe for the untreated and treated  
284 surfaces of the chromitites.

285

286 **Inductively coupled plasma optical emission spectrometry**

287 The elemental concentrations of Mg, Al, Si, Cr, and Fe in the solutions after the  
288 experiment with the chromitite powders were determined with solution-mode inductively coupled  
289 plasma optical emission spectrometry (ICP-OES) at a commercial lab (AGAT labs, Sudbury,  
290 Ontario, Canada). Blanks, sample replicates, duplicates and internal reference materials, both  
291 aqueous and geochemical standards are routinely used in the laboratory as part of the quality  
292 assurance. Tables 2 lists atomic ratios between selected elements in solution and Table A3  
293 their corresponding concentrations.

294

295 **X-ray fluorescence spectroscopy and determination of loss on ignition**

296 The loss on ignition (LOI) for untreated chromitite powders was assessed prior to  
297 analysis by X-ray fluorescence. The LOI gives the proportion of volatile elements or compounds  
298 in a sample (H, H<sub>2</sub>O, S, N) and was determined by heating the sample to 100°C under nitrogen  
299 atmosphere, and to 1000°C under oxygen atmosphere, until a constant wt. % was reached. The  
300 sample was subsequently fused with a borate flux to produce a glass bead for characterization  
301 by X-ray Fluorescence Spectroscopy (XRF). A dilution factor of chromitite to borate flux of 1:24  
302 ensured that no Cr-oxide exsolved from the glass matrix during cooling. The glass bead was  
303 subsequently analyzed with a Panalytical Axios Advanced XRF spectrometer. Table A4 lists the  
304 average concentrations for the major elements in chromitite (on the basis of two  
305 measurements).

306

307 **Scanning electron microscopy, X-ray diffraction (XRD), X-ray fluorescence spectroscopy**

308 Scanning electron microscopy was conducted with a JEOL 6405 at 20 kV, equipped with  
309 both backscattered (BSE) and secondary electron (SE) detectors and an energy dispersive X-  
310 ray spectrometer (EDS). Powder X-ray diffraction of an untreated chromitite samples was done  
311 with a Philips PW 1729 X-ray diffractometer using Cu K $\alpha$  radiation (1.5418 Å) at a voltage and

312 current of 40 kV and 30 mA, respectively. Spectra from powdered samples were collected over  
313 a scan range of 5-75° 2 $\theta$  with a step size of 0.02 °2 $\theta$  and a dwell time of 4 seconds. The XRD  
314 patterns are given in supplementary data A5.

315

316 **Focused ion beam extraction, high-resolution transmission electron microscopy, and**  
317 **scanning transmission electron microscopy**

318 A FEI Helios 600 NanoLab Focused Ion Beam (FIB) microscope, equipped with an *in*  
319 *situ* extraction probe, was used to extract two sections of the sample treated with solution A at  
320 pH 2.5 for subsequent imaging and analyses by TEM. One section was extracted from inside  
321 the chromitite sample, representing an unaltered environment, whereas the other was extracted  
322 from along the altered surface (Schindler et al. 2017). Upon extraction, samples were lifted  
323 using a platinum gas-glue and thinned to electron transparency by ion gas milling (Ga<sup>+</sup> ions).

324 Nanoscale mineralogical and chemical compositions of untreated and treated areas  
325 were characterized using a JEOL 2100 field thermionic emission analytical TEM at the Virginia  
326 Tech National Center for Earth and Environmental Nanotechnology Infrastructure (NanoEarth).  
327 All measurements were taken with an accelerating voltage of 200 kV and a beam current of  
328 approximately 107  $\mu$ A. EDS point analyses and maps were acquired with the instrument  
329 operating in scanning transmission electron microscope (STEM) mode using a JEOL BF  
330 detector, and selected area electron diffraction (SAED) patterns were acquired using a Gatan  
331 Orius SC200D detector.

332

333 **RESULTS**

334 The examined chromitite consists of the major elements Cr, Fe, Mg, Al, Si, O and H,  
335 minor Ti and traces of Ca, Ba, K, Mn, Na and V (Table A4). Elemental ratios relevant to the  
336 following discussion include Cr:Si = 18.7:1, Cr:Al = 4.7:1 and Cr:Fe = 2.13:1. Chromite and  
337 clinocllore are the only two minerals with modal abundances exceeding 1% (on the basis of X-

338 ray powder diffraction). The latter silicate is the most common mineral of the chlorite mineral  
339 group and commonly forms through the chemical alteration of pyroxenes and amphiboles. The  
340 average chemical composition of the clinochlore (on the basis of five analyses with SEM-EDS)  
341 is  $\text{Mg}_3[\text{Si}_4\text{O}_{10}(\text{OH})_2] \times (\text{MgAl}_{1.33}(\text{OH})_6)$ . Areas composed of clinochlore contain an average of 3  
342 wt% Cr (most likely in the form of chromite nanoparticles) with Cr:Si, Cr:Al and Cr:Fe of 1:14,  
343 1:3 and 2.2:1, respectively.

344 The chromite is Mg- and Al-rich and has the average composition ( $\text{Fe}_{0.5}\text{Mg}_{0.5}$ )  
345 ( $\text{Al}_{0.6}\text{Cr}_{1.4}$ ) $\text{O}_4$  ( $N = 5$  with SEM-EDS). On the basis of the average compositions of both minerals  
346 (SEM-EDS) and the bulk composition of the ore sample (XRF), the modal ratio between  
347 chromite and clinochlore is circa 15:1. Chromite occurs as rounded to angular grains in thin  
348 section (Fig. 1a) and is massive in hand samples. Anhedral grains can be up to 5 mm in  
349 diameter and display a cumulate texture. Clinochlore appears colourless, anhedral, and displays  
350 third order interference colours in thin section. The mineral occurs between individual chromite  
351 grains in areas ranging in size from lower ( $\sim 1 \mu\text{m}$ ) to upper micrometers (400-500  $\mu\text{m}$ ) (Fig. 1a).

352 Schindler et al. (2017) showed that clinchlore in chromitite from the Black Thor chromite  
353 deposit contains chromite nanoparticles (Fig. 1b-d). Similar average Cr:Fe in clinochlore (2.2:1,  
354 (SEM-EDS)) and chromite (2.3:1 (SEM-EDS)) suggest that Cr and Fe occur in clinochlore  
355 predominantly as chromite nanoparticles. On the basis of this assumption, the modal ratio  
356 between chromite and clinochlore (15:1) and the average concentration of Cr in clinochlore (3  
357 wt%), the calculated mass ratio between the chromite nanoparticles in clinochlore and the  
358 micrometer-size grains of chromite is circa 1:180.

359

### 360 **The chemical composition of the untreated chromitite surface**

361 Two XPS spectra were taken from areas with a higher and lower proportion of  
362 clinochlore on the surface of an untreated chromitite (Tables 1 and A1). The Cr:Fe varies in the  
363 range of 3.0-3.2 ( $N = 2$ ) to 2.7-3.2 ( $N = 2$ ) in areas containing a lower and higher proportion of

364 clinochlore, respectively. These ratios are higher than those observed by SEM for chlorite  
365 (2.2:1) and chromite (2.3:1) and with XRF for the bulk chromitite sample (2.1:1). Similarly the  
366 average Mg:Si for chromitite determined with XPS (0.7:1) is much lower than the ratio in the  
367 bulk structure (4.7:1). These observations indicate that the sensitivity factors for elements listed  
368 in the database of the Vision software package (which were determined using anhydrous  
369 minerals) are not appropriate to determine exact elemental ratios for spectra of rocks containing  
370 hydrous minerals such as clinochlore. This observation is in agreement with those by Schindler  
371 *et al.* (2009), who showed that the use of the sensitivity factor for Si of 0.325 (Vision 2.2.6) for  
372 hydrated mineral samples (amorphous silica, uranyl minerals) results in larger Si:*M* (*M* = metal)  
373 and Si:O with respect to the bulk composition of the minerals. The authors showed, however,  
374 that relative changes in the elemental ratios determined for hydrous minerals with XPS can be  
375 used to monitor changes in elemental ratios as a function of surface treatment. Hence, changes  
376 in Cr:Si, Cr:Fe and Al:Si between the various dissolution experiments are still considered in this  
377 study (Table 1) as they provide insights into chemical changes on chromitite surfaces under  
378 various conditions.

379

### 380 **Stoichiometric and non-stoichiometric dissolution features on altered chromitite** 381 **surfaces at the micrometer and nanometer scales**

382 Non-stoichiometric dissolution commonly yields altered surfaces that differ in their  
383 chemical composition from the unaltered mineral, whereas stoichiometric dissolution results in  
384 etch features on surfaces with similar elemental ratios as an unaltered surface.

385 Stoichiometric dissolution features occur on the surface of chromite grains. Although  
386 rare, they occasionally occur in the form of symmetrical etch pits (Fig. 2a) and asymmetrical  
387 etch features (Fig. 2b). EDS-SEM chemical distribution maps for Si on a chromitite surface  
388 treated with solution A indicate the occurrence of non-stoichiometric dissolution features on the  
389 surface of clinochlore grains (Fig. 2d). These areas are often highly altered and enriched in Si

390 and depleted in Mg, Al, Fe and Cr (all < 1 wt%) with respect to the chemical compositions of  
391 clinochlore and chromite (Fig. 2c).

392 The absence of diffraction spots and rings in SAED patterns taken from the silica-rich  
393 areas indicate the occurrence of an amorphous silica modification (Schindler et al. 2017). STEM  
394 images indicate the occurrence of fragments of clinochlore in areas composed mainly of silica  
395 (Fig. 3a). Chemical distribution maps for Si, Cr and Mg indicate a higher abundance of chromite  
396 nanoparticles (green) in the clinochlore fragments than in the surrounding silica (Fig. 3b and c).

397

### 398 **Secondary Cr-species on treated chromitite surfaces**

399 The changes in the chemical environments of Cr on the surfaces of the treated  
400 chromitite surfaces can be determined through examination of the binding energies of the  
401 various bands in the Cr 2p<sub>3/2</sub> spectrum (supplementary data B2). The Cr 2p<sub>3/2</sub> spectra taken from  
402 altered chromitite surfaces are shifted to higher binding energy relative to the spectra recorded  
403 from unaltered surfaces (Fig. 4a-c). Spectra with smaller shifts in binding energy display similar  
404 multiplet splitting and peak shape (Fig. 4b), while those with larger shifts in binding energy  
405 depict more asymmetric peak shapes (Fig. 4c). Quantification of the proportions of Cr<sup>3+</sup> and Cr<sup>6+</sup>  
406 species in Cr 2p<sub>3/2</sub> spectra displaying multiplet splitting is complicated by the fact that bands  
407 corresponding to anhydrated and hydrated Cr<sup>3+</sup> and Cr<sup>6+</sup> surface terminations may overlap  
408 (supplementary data B2). However, the identification of the exact nature of the surface  
409 terminations is not a requirement for the quantification of the degree of alteration on a treated  
410 chromitite surface. As indicated in supplementary data B2, the covalency of M-O bonds  
411 decreases with the degree of protonation of the O atom. As such, a higher number of  
412 protonated surface terminations on the chromite surface (i.e., lower electron densities around  
413 the Cr<sup>3+</sup> atoms) results in a shift of the Cr 2p<sub>3/2</sub> spectrum to higher binding energies (Fig. 4-c).  
414 Similarly, a higher number of Cr<sup>6+</sup>-bearing surface terminations would also result in a shift of the  
415 Cr 2p<sub>3/2</sub> spectrum to higher binding energies. Hence, the degree of chromite surface alteration

416 can be related to the abundance of either protonated surface terminations or Cr<sup>6+</sup>-bearing  
417 surface terminations (e.g., <sup>[6]</sup>Cr<sup>3+</sup>-OH<sub>2</sub> or <sup>[4]</sup>Cr<sup>6+</sup>-OH); both such configuration types are defined  
418 here as secondary Cr species, which are presumably absent on the untreated surface.

419 The proportion of secondary Cr species on a treated surface can be calculated from the  
420 weighted average binding energy of the Cr 2p<sub>3/2</sub> spectra (i.e., the total sum of the binding  
421 energies of the bands multiplied by their respective proportions within the envelope), assuming  
422 a linear relationship between the proportions of secondary species on the surface and the  
423 weighted average binding energy. Using this approach, we define the weighted average binding  
424 energy of an untreated chromite surface (577.0 eV) and the average binding energy for Cr<sup>6+</sup>  
425 components (579.4 eV) listed in the NIST database (2012) as the lower (0%) and upper limit  
426 (100%) of secondary Cr-components, respectively. The proportion of secondary Cr-  
427 components, and thus the degree of surface alteration, is then given by the equation

$$428 \quad \text{secondary Cr-components [\%]} = 41 * \text{weighted binding energy Cr 2p spectrum} -$$
$$429 \quad 23694.7 [1]$$

430 where the numbers 41 and 23694.7 are the slope and intersection with the y-axis of the linear  
431 plot, respectively

432

### 433 **Changes in chemical composition on the treated chromitite surfaces: dissolution**

### 434 **features in the absence and presence of bacteria and pyrolusite particles**

435 Quantification of the XPS spectra indicates that treated chromitite surfaces commonly  
436 have lower Cr:Si, Al:Si and Cr:Fe than untreated surfaces (Fig. 5a, Table 1). Surfaces treated  
437 with a TK solution, which contains Fe<sup>2+</sup>, P, and S, have lower Cr:Fe and higher proportions of S  
438 and P than those treated without TK solutions (Table 1). For example, the surface treated with  
439 solution A + bacteria + TK solution (pH 2.3) has the lowest observed Cr:Fe (1.7:1) and the  
440 highest proportion of S and P (Fe:(S+P) is 1.1:1 with P >> S) of all surfaces treated with acidic  
441 solutions (Table 1). The latter surface has also the lowest proportion of secondary Cr species

442 (13%). On the contrary, for all surfaces treated with acidic solutions (either Solution A or TK with  
443 or without bacteria), the final Cr:Si and Al:Si on chromitite are similar (Table 1) and thus, the  
444 addition of cultivated bacteria had a negligible effect on this aspect of the chromitite surface  
445 chemistry.

446 The correlation between Cr:Si and Al:Si indicates that (a) surfaces treated with near-  
447 neutral and alkaline solutions are enriched in Si relative to surfaces either untreated or treated  
448 with acidic solutions, and (b) similar changes in the proportions of Cr and Al relative to Si occur  
449 between surfaces treated with near-neutral and acidic solutions (Fig. 5a). A plot of Cr:Si versus  
450 the proportion of secondary Cr species [%] indicates that the majority of the data follows a linear  
451 trend with higher proportions of secondary Cr species occurring on surfaces with higher Cr:Si  
452 (Fig. 5b). Exceptions to this trend are the surface compositions of the untreated surface (grey  
453 data point) and the surface treated with a  $0.1 \text{ molL}^{-1}$   $\text{MnO}_2$  solution of pH 6.2 (Table 1, Fig. 5b).

454

#### 455 **Proportion of Cr- and Mn-components on the surfaces of $\text{MnO}_2$ particles and chromitites**

456 Optical examinations and XPS spectra recorded after dissolution experiments with  $\text{MnO}_2$   
457 powders show that the proportions of attached pyrolusite particles and Mn on the surfaces of  
458 the chromitite slabs are significantly higher after treatment with near-neutral ( $\text{pH}_{\text{initial}} 6.2$ ) than  
459 after treatment with acidic ( $\text{pH}_{\text{initial}} = 2.5$ ) or alkaline ( $\text{pH}_{\text{initial}} = 8$ ) solutions containing  $0.1 \text{ molL}^{-1}$   
460  $\text{MnO}_2$  (Table 3). XPS studies of pyrolusite particles separated from the chromite powder indicate  
461 the presence of detectable amounts of Cr- Fe-, Si- and Al-bearing species (or particles) on the  
462 surfaces of the pyrolusite grains. For example, concentrations of Cr on the surface of the  
463 pyrolusite particles can be up to 8.3 at% Cr, whereby the Cr:Fe on the respective surfaces  
464 (2.0:1-2.8:1) are similar to the ratio on the untreated chromitite surface (Tables 1 and 3).

465

466

467

## 468 **Microbial community composition in dissolution treatments**

469 The initial microbial inoculum was a known mixed community containing at least 60%  
470 Fe-oxidizing bacteria including *Acidithiobacillus ferrooxidans*, *Alicyclobacillus* sp. and acidophilic  
471 heterotrophs including *Acidiphilium* sp. The 1 mL inoculums that were added with and without  
472 TK solution B were sampled at the end of the dissolution experiment. Only the solution from  
473 1mL bacteria + TK full solution had sufficient biomass to extract DNA with a yield of 2.3 ng $\mu$ L<sup>-1</sup>.  
474 The community profile indicated a loss of most of the Fe-oxidizing bacteria (supplemental Table  
475 A6) (0.1% abundance of *Alicyclobacillus* sp. remained) with the vast majority of the community  
476 represented by heterotrophic acidophiles, > 98% *Acidiphilium* sp. This indicates that no Fe- or  
477 S- oxidizing chemolithotrophs were sustained through the duration of the experiment and the  
478 population likely declined after the Fe<sup>2+</sup> from the TK media was consumed.

479

## 480 **Chemical composition of the solutions after the experiments**

481 Linear correlations are observed between the elemental concentrations of Al and Cr  
482 (Fig. 6a) and Si and Cr (Fig. 6b), with the highest concentration of Cr consistently occurring in  
483 solutions treated with the acidic solution A (Table A3). In both correlations, concentrations of Cr  
484 in solutions containing pyrolusite particles are below the observed trend. Table 2 lists the Cr:Al,  
485 Cr:Fe and Cr:Si in chromitite and clinocllore as well as in the final solutions; however, the Cr:Fe  
486 is only meaningful for experiments in which additional Fe<sup>2+</sup> was not introduced (i.e., those  
487 without TK and bacteria solutions). Closer inspection of Cr:Al, Cr:Fe and Cr:Si in the solutions  
488 shows that dissolution of chromitite was non-stoichiometric in all dissolution experiments, with  
489 all solutions being enriched in Si relative to the Si:Cr in the bulk material (Table 2). It is also  
490 apparent that Cr:Al and Cr:Fe in solutions after experiments carried out under acidic conditions  
491 and deionized water, respectively, are similar to those observed in clinocllore.

492

493

494 **DISCUSSION**

495 Laarman (2013) described the abundance, morphology and chemical composition of chlorite  
496 group minerals from the Black Label, Black Thor and Big Daddy chromite deposits. The author  
497 argues that these minerals are the product of retrogressive, hydrothermal alteration of chromite  
498 and amphiboles and that the Mg, Al and Cr contents of clinocllore reflect that of the primary  
499 chromite. For example, chlorites with elevated Cr<sub>2</sub>O<sub>3</sub> either replace Cr-rich tremolite, occur as  
500 interstitial material in massive chromitites, or occur in fractures where Cr becomes relatively  
501 mobile with fluid influx. Laarman (2013) also reports that in minerals of the chlorite group, the  
502 Cr<sub>2</sub>O<sub>3</sub> concentration ranges from 1 to 10 wt%, with minerals occurring in fractures having the  
503 highest concentrations of Cr.

504 The identification of chromite nanoparticles in clinchlore by Schindler et al. (2017)  
505 suggests that the high Cr contents in many chlorites at the Black Label, Black Thor and Big  
506 Daddy chromite deposits are the result of the presence of these nanoparticles and not as  
507 commonly assumed a result of the replacement of Al<sup>3+</sup> by Cr<sup>3+</sup> in the structure of minerals of the  
508 chlorite group (Lapham 1958).

509 In the next sections, we will address first non-stoichiometric dissolution features  
510 observed on the surfaces of the treated chromitites, followed by discussions on the occurrence  
511 of surficial secondary Cr-species, links between the chemical compositions of surfaces and  
512 solutions and the effect of pH, pyrolusite particles and bacteria on the degree of chromitite  
513 dissolution.

514

515 **Non-stoichiometric dissolution of chromitite**

516 Both major constituents of chromitite, chromite and clinocllore, appear to undergo non-  
517 stoichiometric dissolution under the investigated conditions. According to Zhang et al. (2016),  
518 the non-stoichiometric dissolution of chromite, especially under strongly oxidizing conditions,  
519 results in the removal of Cr as Cr<sup>6+</sup><sub>(aq)</sub> and in the re-precipitation of Fe<sup>2+</sup><sub>(aq)</sub> as Fe<sup>3+</sup>-hydroxides.

520 Evidence for a similar mechanism on the chromitite surfaces treated with near-neutral and  
521 alkaline solutions is seen in lower Cr:Fe and Cr:Al values relative to the untreated surface  
522 (Table 1), which are consistent with the presence of Fe- and Al-hydroxide species precipitated  
523 or adsorbed to the chromitite surface.

524 Micrometer-thick silica-enriched surfaces are visible by SEM (Fig. 2d) on surfaces of  
525 clinocllore grains after treatment under acidic (but not near-neutral) pH conditions. This  
526 observation is in accord with previous observations on the formation of silica-rich surfaces on  
527 chlorite-group minerals treated with acidic solutions (Brandt et al. 2003) and on chromitite  
528 samples treated with sulfuric acid solutions at higher  $T$  (Zhao et al. 2014). As the sole possible  
529 source of Si in the studied system is clinocllore, the occurrence of the Si-rich layer indicates  
530 complete dissolution of clinocllore followed by re-precipitation of amorphous silica within an  
531 interfacial fluid film on the surface of the mineral (Hellman et al. 2002, 2012, Putnis and Ruiz-  
532 Aguda 2013).

533 The solubilities of clinocllore and chromite are significantly different in aqueous  
534 solutions. Chromite is a refractory mineral and sparingly soluble at room temperature, whereas  
535 the solubility of chlorite group phases depends on solution pH and the activities of its constituent  
536 ions. In a natural environment, the latter may be largely controlled by the presence of secondary  
537 minerals such as gibbsite and kaolinite (Kittrick 1982). The absence of these minerals and their  
538 higher solubility in an acidic environment (e.g., pH 2-3) suggest that the dissolution of  
539 clinocllore has been likely controlled by the solubility of amorphous silica in the experiments  
540 under acidic pH conditions (pH = 2-3, Faure 1998). The effect of the higher solubility of  
541 clinocllore relative to chromite is consistent with the final Cr:Si ratios observed in the reacted  
542 solutions (Table 2). The mean Cr:Si in solution is 1:7.7, which is much closer to the value  
543 measured in clinocllore (1:14) than that measured in the bulk chromitite (18.7:1; Table 2).

544 The occurrence of a visible layer of amorphous silica at low pH indicates the formation of  
545 a higher proportion of amorphous silica on the surface of chromitites treated under acidic than

546 near neutral pH conditions. However, higher concentrations Si in solution after the experiments  
547 under acidic conditions (Table 2) indicate that the re-precipitation of amorphous silica is not a  
548 complete reaction (most likely due to the high solubility of amorphous silica, Faure 1998).  
549 Hence, with increasing dissolution of clinocllore, the total amount of Cr and Fe on the chromitite  
550 surface remains relatively constant (due to the low solubility of chromite), while the total  
551 amounts of Al, Si and Mg on the treated surfaces decrease. As the loss of Al on the surface is  
552 somewhat mitigated by the relatively insoluble chromite, the loss of Si is greater, resulting in the  
553 observed increases in Al:Si and Cr:Si with decreasing pH value in solution (Fig. 5a, Table 1).

554

### 555 **Secondary Cr species on treated chromitite surfaces of treated chromitites**

556 Figure 5b shows an increase in the proportions of secondary Cr species on chromite  
557 with increasing dissolution of the chromitite (the latter increases as a function of Cr:Si ). An  
558 exception to this trend is the chromitite surface treated with a  $0.1 \text{ molL}^{-1}$   $\text{MnO}_2$  solution ( $\text{pH}_{\text{initial}} =$   
559 6.2; Table 1). This surface has the lowest Cr:Si of all treated surfaces (even lower than that  
560 treated with deionized water), but the proportion of secondary Cr species approximates that of  
561 surfaces treated with acidic solutions (Table 1, Fig. 5b).

562 A likely reason for this observation is the presence of a high proportion of pyrolusite  
563 particles on the surface of the chromitite after the experiment (Table 3). Particle attachment to  
564 mineral surfaces is favored where surfaces and particles have opposing electrostatic charges.  
565 The points of zero charge (PZC) for amorphous silica, clinocllore, pyrolusite and Al-rich  
566 chromite are 4.1, 4.7, 5.9 and 7.4 respectively (Kosmulski 2009a, b; Alvarez-Silva 2010;  
567 Christiano et al. 2011). Hence in a solution of pH 6.2, the surfaces of amorphous silica, and  
568 clinocllore are negatively-charged, surfaces of pyrolusite are slightly negatively-charged, and  
569 those of chromite are slightly positively-charged and the attachment of pyrolusite particles to the  
570 surface of chromite is thus favored at pH 6.2.

571 The presence of pyrolusite particles on the surface of chromitite may also be related to  
572 particle agglomeration and aggregation. Agglomeration is commonly favored when the surface  
573 of the particles has a minimum charge, which is the case when either (1) the pH is close to the  
574 PZC, or (2) when adsorbed species neutralize positive or negative surface charges (e.g., Hotze  
575 et al. 2010). The surface charges listed above indicate that attachment, agglomeration, and  
576 heteroaggregation of pyrolusite particles on the surface of chromite is favored in the solution of  
577  $\text{pH}_{\text{initial}} = 6.2$ , as compared to the solutions of  $\text{pH}_{\text{initial}} = 2.5$  and 8.0, in accord with the  
578 observations in this study (Table 3).

579 The higher abundance of pyrolusite particles on the surface of chromitite treated with a  
580 solution of  $\text{pH}_{\text{initial}} = 6.2$  likely provided a higher number of adsorption sites for aqueous species  
581 such as  $\text{Cr}(\text{OH})^{2+}$  and  $\text{Cr}(\text{OH})_2^+$ , which are the predominant  $\text{Cr}^{3+}$ -bearing aqueous species in  
582 weakly acidic conditions (Fendorf 1995). The presence of such species on the surface of the  
583 attached pyrolusite particles may explain the observed elevated proportions of secondary Cr  
584 species on the chromitite surface treated with a  $0.1 \text{ mol L}^{-1}$   $\text{MnO}_2$  solution of pH 6.2 (Fig. 5b).

585 Chromate species such as  $(\text{HCr}^{6+}\text{O}_4)^-$  and  $(\text{Cr}^{6+}\text{O}_4)^{2-}$  form predominantly under alkaline  
586 pH conditions in solution but can also form through oxidation of  $\text{Cr}^{3+}$  by  $\text{Mn}^{3+}/\text{Mn}^{4+}$ -bearing Mn-  
587 oxides under acidic conditions (Eary and Rai 1987, Fendorf 1995). The occurrence of adsorbed  
588 chromate species on the surface of the treated chromitite cannot be completely ruled out  
589 because Al-rich chromite and Fe-hydroxide species (or precipitates) that form during dissolution  
590 experiments with  $\text{CaCO}_3$ -bearing solutions have net-positive surface charges under acidic to  
591 near-neutral pH-conditions, which would promote the adsorption of the negative charged  
592 chromate species.

593 The observation that no Fe- and S-oxidizing bacteria were sustained during the  
594 dissolution experiments indicates that the bacteria were either (1) not resistant to the presence  
595 of  $\text{Cr}^{6+}$  aqueous species, or (2) did not gain enough energy from the potential oxidation of  
596 released  $\text{Fe}^{2+}$  and  $\text{Cr}^{3+}$  species. This observation may explain the similarities in the proportions

597 of secondary Cr-species after the dissolution experiments under acidic conditions in the  
598 presence and absence of bacteria (Table 1, Fig. 5b).

599

600 **Linking surface composition of chromitite slabs and pyrolusite particles with the**  
601 **chemical composition of solutions**

602 Comparison between the compositions of surfaces (chromitite and pyrolusite) and  
603 solution shows that the concentrations of Cr in solution are controlled by (1) the initial release of  
604 chromite nanoparticles during clinocllore dissolution, (2) the adsorption of chromite  
605 nanoparticles (and other Cr-bearing aqueous species) to the surfaces of pyrolusite particles,  
606 and (3) the potential oxidation of  $\text{Cr}^{3+}$  to  $\text{Cr}^{6+}$ .

607 In addition to the formation of silica-enriched surface layers during dissolution/re-  
608 precipitation processes, the dissolution of clinocllore will likely release chromite nanoparticles to  
609 solution. This conclusion is in accord with the following four considerations and/or observations:

- 610 (1) In a dissolution-re-precipitation process, all components (including chromite  
611 nanoparticles) are initially removed from the surface;
- 612 (2) The highly hydrous and porous character of the hydrous silica layer easily allows the  
613 diffusion and transport of aqueous species and nanoparticles (Schindler et al 2009c;  
614 Putnis and Ruiz-Aguda 2013, Schindler and Hochella 2017);
- 615 (3) Chromite nanoparticles occur in lower abundance in the hydrous amorphous silica layer  
616 relative to the unaltered clinocllore grain (Fig. 3b and c, Schindler et al. 2017);
- 617 (4) Elevated Cr:Si in acidic, as opposed to near-neutral and alkaline solutions likely result  
618 from (a) a higher release rate of chromite nanoparticles and (b) a higher degree of  
619 alteration of the surficial chromite grains (higher proportion of secondary Cr species)  
620 (Table 2, Fig. 5b).

621 In experiments with pyrolusite particles present, solutions are depleted in Cr, relative to  
622 Al and Si (Fig. 6a-b) with Cr:Al and Cr:Si as low as 1:8.4 and 1:145, respectively (Table 2). This

623 depletion in Cr and Cr:Fe of 2:1 to 3:1 on the surfaces of the pyrolusite particles suggest  
624 preferential sequestration of chromite nanoparticles over Al- and Si-bearing aqueous species by  
625 the pyrolusite particles (Table 3). Conversely, similar Cr:Al in acidic solutions and a similar  
626 Cr:Fe in deionized water as in clinochlore indicate that neither Cr, Al, nor Fe have been  
627 preferentially removed from the respective solutions through adsorption and precipitation  
628 processes.

629 In solutions after experiments with  $\text{CaCO}_3$  in solution, Cr:Al and Cr:Fe are greater than  
630 those in the initial clinochlore (Table 2). This indicates an enhanced adsorption or precipitation  
631 of Al and Fe-species under alkaline pH conditions (see above). Preferential adsorption or  
632 precipitation of Al and Fe relative to Cr occurs commonly when Cr is in the hexavalent oxidation  
633 state, as the geochemical and crystal chemical properties of  $\text{Cr}^{3+}$  are sufficiently similar to those  
634 of  $\text{Al}^{3+}$  and  $\text{Fe}^{3+}$  to not result in a significant difference in their environmental fate (Fendorf  
635 1995). Although the XPS studies could not unequivocally identify  $\text{Cr}^{6+}$  species on the surfaces of  
636 the altered chromitites, the latter conclusion is in accord with the observed higher stability of  
637 chromate aqueous species under alkaline pH conditions (Fendorf 1995; Zhang et al. 2016).

638 In conclusion, chemical and mineralogical features on the surfaces of chromitite and  
639 pyrolusite particles and the compositions of the respective solutions show that the  
640 concentrations of Cr in solution are controlled by the release of chromite nanoparticles, the  
641 adsorption of chromite nanoparticles or Cr-bearing aqueous species to the surfaces of  
642 pyrolusite particles and the potential oxidation of  $\text{Cr}^{3+}$  to  $\text{Cr}^{6+}$ .

643

#### 644 **Effect of the pH, solution composition and bacteria on the degree of chromitite** 645 **dissolution**

646 The occurrence of multiple chemical and physical processes on the surfaces of the  
647 treated chromitites makes evaluating the combined effects of solution composition, pH and  
648 bacteria presence on the degree of dissolution of chromitite difficult. The higher concentrations

649 of Cr and more pronounced dissolution features on the chromitite slabs after the dissolution  
650 experiments under acidic than under neutral or weak basic conditions indicate that a decrease  
651 in pH likely enhances the degree of dissolution and the release of associated chromite  
652 nanoparticles. This is supported by the observations that the formation of silica-rich alteration  
653 layers on silicate minerals is commonly favoured under acidic rather than near neutral and  
654 alkaline pH conditions (e.g. Brantley 2003). Higher concentrations of Cr after dissolution  
655 experiments in solution A (sulfate-phosphate-bearing solution without  $\text{Fe}^{2+}$ ) than in solution TK  
656 (Fig. 6, Table A3) suggest that the absence of  $\text{Fe}^{2+}$ -bearing aqueous species (and thus a higher  
657 degree of undersaturation with respect to chromite; Table A1) has an effect on the degree of  
658 dissolution. However, this is not apparent when considering the respective compositions of the  
659 treated slabs (where higher Cr:Si and higher proportions of secondary Cr species occur after  
660 the experiments with the TK solution than solution A, Table 1).

661 The role of bacteria is also unclear during these dissolution experiments as their  
662 abundances seem to be controlled primarily by the initial amount of  $\text{Fe}^{2+}$  in solution rather than  
663 by the amount of  $\text{Fe}^{2+}$  released during the dissolution of the chromite nanoparticles.

664

## 665 **IMPLICATIONS**

666 Evaluation of the potential fate of Cr in contaminated soils, tailings, and waste rock piles  
667 is a complex issue requiring a thorough characterization of the mechanisms in operation during  
668 the non-stoichiometric dissolution of chromitite ore. An understanding of these dissolution  
669 mechanisms is fundamental to being able to accurately predict (1) the compositional evolution  
670 of aqueous solutions in contact with chromitite, particularly related to formation of the highly-  
671 toxic chromate  $\text{Cr}^{6+}$  species; (2) the compositional, structural, and mineralogical changes  
672 occurring on the surface of the affected minerals (i.e., clinocllore and chromite); and (3) the  
673 behaviour of nanoparticles upon their release from the dissolving clinocllore phase, thereby  
674 affecting the transport, reactivity, and bioavailability of chromium.

675 Elucidation of dissolution features of chromitite is facilitated in this study by a multi-  
676 analytical approach, utilizing methods capable of nano-scale imaging and chemical  
677 characterization such as XPS, SEM and TEM. The comprehensive data set collected here  
678 shows the importance of factors such as dissolution rates of Cr-bearing silicates and chromite,  
679 the release of chromite nanoparticles, re-precipitation of amorphous silica, the pH-dependence  
680 adsorption (or precipitation) of Fe- and Al-bearing hydroxides and sulfates. It also shows that  
681 chemical signatures of aqueous solutions in contact with chemically complex rocks such as  
682 chromitite can be only explained when considering physical, chemical and mineralogical  
683 characteristics of each phase present in the rock. Bacterial activities and species appear to  
684 have no direct effect on the release of Cr species or on the surface composition of altered  
685 chromitites. However, their presence in tailings, mine waste piles and soils may control pH and  
686 Eh due to their ability to either oxidize or reduce redox-sensitive ions such as  $S^{2-}$ ,  $(SO_4)^{2-}$ ,  $Fe^{2+}$ ,  
687  $Fe^{3+}$ ,  $Mn^{2+}$  and  $Mn^{4+}$  and thus control indirectly degrees of chromitite alteration and the  $Cr^{3+}:Cr^{6+}$   
688 redox-chemistry in solution.

689 The existence of chromite nanoparticles in silicate minerals associated with chromite  
690 deposits at the Ring of Fire in Ontario, Canada and the Mistake mine in California, USA  
691 suggests a widespread occurrence of chromite nanoparticle in Cr-rich rocks and minerals. The  
692 ultimate release of these nanoparticles during either natural weathering or mine-related rock  
693 processing and waste disposal may, therefore, be a significant vector of chromium introduction  
694 into the environment. Here, we show that the magnitude of this release can only be assessed by  
695 considering the dominant geochemical conditions (e.g., pH, Eh, and counter-ion chemistry) that  
696 are driving chromitite dissolution and re-precipitation and adsorption processes. The  
697 observations in this study suggest that release of chromite nanoparticles during alteration of  
698 chromitite ore fragments in future mine tailings would be favoured at low pH values in a sulfide-  
699 rich environment as acidic pH conditions favour the non-stoichiometric dissolution of the  
700 associated Cr-silicates. The results of this study also suggest that released chromite

701 nanoparticles will be effectively sequestered by larger colloids or particles in pore solutions  
702 within mine tailings settings. Neutralization of acidic pore solutions towards near neutral pH  
703 conditions through liming and the use of barriers or linings composed of clays or hydroxides  
704 should be then sufficient to limit the amount of chromite nanoparticles released into the  
705 environment. Further work would be required to assess the ability of chromite nanoparticles to  
706 ultimately control the abundance of  $\text{Cr}^{6+}_{(aq)}$  in soils and outcrops proximal to mining activities  
707 and tailings.

### 708 **ACKNOWLEDGEMENTS**

709 This work was supported by a Best of Science Award from the Ministry of Environment and  
710 Climate Change of Ontario to MS, as well as by the Virginia Tech National Center for Earth and  
711 Environmental Nanotechnology Infrastructure (NanoEarth), a member of the National  
712 Nanotechnology Coordinated Infrastructure (NNCI) funded by NSF (ECCS 1542100). We also  
713 thank Professor G. Parthasarathy and an anonymous reviewer for their comments on earlier  
714 version of the paper, Associate Editor David Singer for handling the paper and Christopher  
715 Winkler, James Tuggle, and the Nanoscale Fabrication and Characterization Laboratory, a  
716 portion of the Institute for Critical Technology and Applied Science at Virginia Tech for their  
717 technical assistance.

### 718 **REFERENCES**

- 720 Bartlett, R.J. and James, B.R. (1979) Behavior of chromium in soils: III. Oxidation. *Journal of*  
721 *Environmental Quality* 8, 31–35.
- 722 Brandt, F., Bosbach, D., Krawczyk-Barsch, E., Arnold, T. and Bernhard G. (2003) Chlorite  
723 dissolution in the acid pH-range: A combined microscopic and macroscopic approach.  
724 *Geochimica et Cosmochimica Acta* 67, 1451–1461.
- 725 Brantley, S.L. 2003. 5.03-Reaction kinetics of primary rock-forming minerals under ambient  
726 conditions. *Treatise on Geochemistry* 5. 73-117. Eary, L.E. and Rai, D., (1987) Kinetics

- 727 of chromium(III) oxidation to chromium(VI) by reaction with manganese dioxide.  
728 Environmental Science and Technology 21, 1187–1193.
- 729 Fandeur, D., Juillot, F., Morin, G., Olivi, L., Cognigni, A., Ambrosi, J.P., Guyot, F. and Fritsch, E.  
730 (2009) Synchrotron-based speciation of chromium in an Oxisol from New Caledonia:  
731 importance of secondary Fe-oxyhydroxides. American Mineralogist 94, 710–719.
- 732 Fendorf, S.E. (1995) Surface reactions of chromium in soils and waters. Geoderma 67, 55–71.
- 733 Faure, G. (1998) Principles and Applications of Geochemistry. 2<sup>nd</sup> Edition, Prentice Hall, New  
734 Jersey, USA.
- 735 Gustafsson, J.P. (2012) Visual MINTEQ, ver. 3.0. KTH Department of Land and Water  
736 resources engineering, Stockholm, Sweden.
- 737 Hellmann, R., Penisson, J-M, Hervig, RL, Thomassin, J.H. and Abrioux, M.F. (2003) An  
738 EFTEM/HRTEM high-resolution study of the near surface of labradorite feldspar altered  
739 at acid pH: evidence for interfacial dissolution-reprecipitation. Physics and Chemistry of  
740 Minerals 30: 192-197.
- 741 Hellmann R., Wirth, R., Daval, D., Barnes, J-P., Penisson, J-M., Tisserand, D., Epicier, T.,  
742 Florin, B. and Hervig, R.L. (2012) Unifying natural and laboratory chemical weathering  
743 with interfacial dissolution–reprecipitation: A study based on the nanometer-scale  
744 chemistry of fluid–silicate interfaces. Chemical Geology 280, 1-2.
- 745 Hotze, E.M. Phenrat, T. and Lowry, G.V. (2010) Nanoparticle Aggregation: Challenges to  
746 Understanding Transport and Reactivity in the Environment. Journal of Environmental  
747 Quality 39, 1909–1924.
- 748 Hseu, Z.Y. and Iizuka, Y. (2013) Pedogeochemical characteristics of chromite in a paddy soils  
749 derived from serpentinites. Geoderma 202–203, 126–133.
- 750 Izbicki, J.A., Ball, J.W., Bullen, T.D. and Sutley, S. (2008) Chromium, chromium isotopes and  
751 selected traced elements, western Mojave Desert, USA. Applied Geochemistry 23,  
752 1325–1352.

- 753 Kamaludeen, S. P. B. Megharaj, M., Juhasz, A.L., Sethunathan, N. and Naidu, R. (2003)  
754 Chromium–Microorganism Interactions in Soils: Remediation Implications. Reviews of  
755 Environmental Contamination and Toxicology 178, 93–164.
- 756 Kittrick, J.A. (1982) Solubility of two high-Mg and two high-Fe chlorites using multiple equilibria.  
757 Clays and Clay Minerals 30, 167-179.
- 758 Kien, C.N., Noi, N.V., Son, L.T. Ngoc, H., Tanaka, S., Nishina, T. and Iwasaki, K. (2010) Heavy  
759 metal contamination of agricultural soils around a chromite mine in Vietnam. Soil  
760 Science and Plant Nutrition 56, 344–356
- 761 Kosmulski, M. (2009a) pH-dependent surface charging and points of zero charge. IV. Update  
762 and new approach. Journal of Colloid and Interface Science 337, 439-448
- 763 Kosmulski, M. (2009b) Surface Charging and Points of Zero Charge. CRC press, Taylor &  
764 Francis group, ISBN 978-1-4200-5188-9.
- 765 Lapham, D. M. (1958) Structural and chemical variation in chromium chlorite: American  
766 Mineralogist 43, 921-956.
- 767 Laarman, J.E. (2013) Detailed metallogenic study of the McFaulds lake chromite deposits,  
768 Norther Ontario, Ph.D. thesis, The University of Western Ontario, pp. 494,
- 769 Morrison J.M., Goldhaber, M.B., Mills C.T., Breit G.N., Hooper, R.L., Holloway, J.M., Diehl, S.F.  
770 and Ranville, J.F. (2015) Weathering and transport of chromium and nickel from  
771 serpentinite in the Coast Range ophiolite to the Sacramento Valley, California, USA  
772 Applied Geochemistry 61, 72–86.
- 773 NIST X-ray Photoelectron Spectroscopy Database (2012) NIST Standard Reference Database  
774 20, Version 4.1, <https://srdata.nist.gov/xps/>.
- 775 Oze, C., Bird, D.K. and Fendorf, S. (2007) Genesis of hexavalent chromium from natural  
776 sources in soil and groundwater. Proceeding of the National Academy of Science USA  
777 104, 6544–6549.

- 778 Oze, C., Fendorf, S., Bird, D.K. and Coleman, R.G. (2004) Chromium geochemistry in  
779 serpentinized ultramafic rocks and serpentine soils from the Franciscan complex of  
780 California. *American Journal of Sciences* 304, 67–101.
- 781 Parthasarathy, G., Choudary, B.M., Sreedhar, B., Kunwar, A.C. and Srinivasan, R. (2003)  
782 Ferrous saponite from the Deccan Trap, India, and its application in adsorption and  
783 reduction of hexavalent chromium. *American Mineralogist* 88, 1983-1988.
- 784 Pillay, K. von Blottnitz, H. and Petersen, J. (2003) Ageing of chromium(III)-bearing slag and its  
785 relation to the atmospheric oxidation of solid chromium(III)-oxide in the presence of  
786 calcium oxide. *Chemosphere* 52, 1771–1779.
- 787 Putnis CV and Ruiz-Aguda E (2013) The Mineral–Water Interface: Where Minerals react with  
788 the Environment. *Elements*: **9**, 177–182.
- 789 Souza, R.F., Paulo R.G. Brandão, P.R.G. and Paulo, J.B.A. (2012) Effect of chemical  
790 composition on the  $\zeta$ -potential of chromite. *Minerals Engineering* 36–38, 65–74.
- 791 Schindler, M., Hawthorne, F.C., Freund, M.S , and Burns, P.C. (2009a): XPS spectra of uranyl  
792 minerals and synthetic compounds I. The U 4f spectrum. *Geochimica et Cosmochimica*  
793 *Acta* 73, 2471-2487.
- 794 Schindler, M., Hawthorne, F.C., Freund, M.S, and Burns, P.C. (2009b): XPS spectra of uranyl  
795 minerals and synthetic compounds II. The O1s spectrum. *Geochimica Cosmochimica*  
796 *Acta* 73, 2488-2509.
- 797 Schindler, M., Durocher, J., Abdu, Y., and Hawthorne, F.C. (2009c) Hydrrous Silica Coatings:  
798 Occurrence, Speciation of Metals, and Environmental Significance. *Environmental*  
799 *Science and Technology* 43, 8775–8780.
- 800 Schindler, M., Berti, D. and Hochella Jr. M.F. (2017) Previously unknown mineral-nanomineral  
801 relationships with important environmental consequences: The case of chromium  
802 release from dissolving silicate minerals. *American Mineralogist* (submitted)

- 803 Schindler, M. and Hochella Jr. M.F. (2017) Sequestration of Pb- Zn- Sb- and As-bearing  
804 incidental nanoparticles by mineral surface coatings and mineralized organic matter in  
805 soils. Environmental Science: Processes & Impacts (submitted)
- 806 Schweda, P., Sjöberg L., and Södervall U. (1997) Near-surface composition of acid-leached  
807 labradorite investigated by SIMS. Geochimica et Cosmochimica Acta 61, 1985–1994.
- 808 Stott, G.M., Corkery, M.T., Percival, J.A., Simard, M. and Goutier, J. (2010) A revised terrane  
809 subdivision of the Superior Province; Summary of Field Work and Other Activities 2010,  
810 Ontario Geological Survey, Open File Report 6260, p. 20-1–20-10.
- 811 Tiwary, R.K., Dhakate, R., Rao, V.A. and Singh, V.S. (2005) Assessment and prediction of  
812 contaminant migration in ground water from chromite waste dump Environmental  
813 Geology (2005) 48: 420–429.
- 814 Tuovinen, O.H. and Kelly, D.P. (1974) Studies on the Growth of Thiobacillus ferrooxidans IV.  
815 Influence of Monovalent Metal Cations on Ferrous Iron Oxidation and Uranium Toxicity  
816 in Growing Cultures Archives of Microbiology 98, 167-174.
- 817 Wagner, C.D., Riggs, W.M., Davis, L.E., Moulder, J.F. (1979) Handbook of X-ray photoelectron  
818 spectroscopy, Perkin Elemer, INC., Waltham, MA, USA, 1<sup>st</sup> edition.
- 819 Weaver, R.M. and Hochella, M.F. Jr. (2003) The reactivity of seven Mn-oxides with Cr<sup>3+</sup>aq: A  
820 comparative analysis of a complex, environmentally important redox reaction. American  
821 Mineralogist 88, 2016–2027.
- 822 Weston R. and Shinkle D.A. (2013) Geology and stratigraphy of the Black Thor and Black Label  
823 chromite deposits, James Bay Lowlands, Ontario, Canada 12th SGA Biennial Meeting  
824 Proceedings.
- 825 Wood, W.W., Clark, D., Imes, J.L. and Councill, T.B. (2010) Eolian transport of geogenic  
826 hexavalent chromium to ground water. Ground Water 48, 19–29.
- 827 Zhang, B., Shi, P. and Jiang, M. (2016) Advances towards a Clean Hydrometallurgical Process  
828 for Chromite. Minerals 2016, 6, 7; 12p.

829 Zhao, Q., Liu, C.J., Shi, P.Y., Zhang, B., Jiang, M.F., Zhang, Q.S. and Zevenhoven, H.S.R.  
830 Sulfuric acid leaching of South African chromite. Part 1: Study on leaching behavior.  
831 International Journal of Mineral Processing 130, 95-101.

832

### 833 FIGURE CAPTIONS

834 Figure 1 (a) SEM image of chromitite from the Black Thor chromite deposit, the occurrence of  
835 clinochlore in the interstices of chromite grains is indicated with arrows; (b) TEM image of the  
836 clinochlore matrix indicating the presence of chromite nanoparticles; (c) high-resolution TEM  
837 images of an individual chromite nanoparticle depicting lattice fringes with  $d = 2.05 \text{ \AA}$  (400); (d)  
838 SAED pattern of clinochlore indicating the presence of a single crystal of clinochlore (diffraction  
839 spots) and chromite nanoparticles (diffraction rings).

840

841 Figure 2 (a) SEM image in BSE mode of a nearly symmetrical etch pit on the surface of a  
842 chromite grain treated with a bacteria + TK solution of pH 2.0; (b) SEM image in BSE mode of  
843 asymmetric etch features along an edge of a chromite grain after treatment with solution A of pH  
844 2.5; (c)-(d) BSE image in BSE mode and corresponding chemical distribution map for Si of a  
845 chromitite grain treated with solution A of pH 2.5; highly-altered clinochlore and silica-rich  
846 patches on the chromitite surface are indicated with arrows.

847

848 Figure 3 (a) STEM image of a selected area in a FIB section extracted from a surface treated  
849 with solution A at pH 2.5; areas composed of chromite, clinochlore and amorphous silica are  
850 labelled accordingly, a fragment of clinochlore within the amorphous silica matrix depicted in (b)  
851 and (c) is encircled; (b)-(c) STEM-EDS chemical distribution maps for (b) Si (red) and Cr (green)  
852 and (c) Mg (blue) and Cr (green).

853

854 Figure 4 Cr 2p<sub>3/2</sub> spectra for various chromitite surfaces: (a) untreated; (b) treated with a bacteria  
855 + TK solution; (c) treated with a 0.1 molL<sup>-1</sup> MnO<sub>2</sub> solution; a vertical grey-shaded bar indicates  
856 the location of the peak at the lowest binding energy of the spectrum for the untreated surface.

857

858 Figure 5 (a) plots of the Cr:Si versus Al:Si determined with XPS for untreated (grey data point)  
859 and treated (black data points) chromitite surfaces; (b) Cr:Si versus proportion of secondary Cr  
860 species on the surface of untreated (grey data point) and treated surfaces, , data points  
861 representing surfaces treated with acidic solutions in the presence and absence of bacteria are  
862 indicated with black squares and circles, respectively; data points representing surfaces treated  
863 with near neutral and alkaline solutions are depicted with black triangles pointing up and down,  
864 respectively.

865

866 Figure 6 (a)-(d) plots with the concentrations of (a) Al versus Cr and (b) Si versus Cr in solutions  
867 after experiments with chromitite powders; solid lines indicates calculated linear regression  
868 curves; symbols for data points are the same as for Figure 5

869

870

871

872

873

874

875

876

877

878

879

880

881

882

883

884

885

886

887

888

889

890 Table 1 Results from dissolution experiments with chromitite slabs (0.5 x 0.5(1) x 0.1cm) in 25 mL solution for four weeks: selected  
 891 elemental ratios between major elements and proportion of secondary Cr species on the surface of the treated samples determined  
 892 with XPS after the experiment; N (XPS): number of spectra taken from the surface; the uncertainty of the pH and Eh (mV) is  $\pm 0.1$

Experiment	Cr:Si	Cr:Fe	Al:Si	Fe:(P+S)	Secondary Cr species [%]	N XPS	pH <sub>initial</sub> pH <sub>end</sub>	Eh <sub>initial</sub> Eh <sub>initial</sub>
Untreated	1.8:1	3.0:1	2.1:1	n.a.	0	4		
1 mL bacteria TK + 24 mL TK	1.4:1	2.0:1	1.8:1	2.4 S >> P	19	2	2.3 <sub>initial</sub> 2.4 <sub>end</sub>	0.6 0.5
25 mL TK	1.3:1	1.9:1	1.6:1	2.0 S >> P	17	2	2.3 <sub>initial</sub> 2.4 <sub>end</sub>	0.6 <sub>i</sub> 0.5
25 mL solution A	1.3:1	3.5:1	1.4:1	2.4 S ~ P	15	2	2.5 <sub>initial</sub> 2.6 <sub>end</sub>	0.6 0.5
1 mL bacteria TK + 24 mL solution A	1.2:1	1.7:1	1.5:1	1.1 P >> S	13	2	2.3 <sub>initial</sub> 2.4 <sub>end</sub>	0.6 0.5
deionized water	1.1:1	2.25:1	1.5:1	n.a.	6	2	7 6.7 <sub>end</sub>	0.6 0.5
25 mL Solution A 0.1 molL <sup>-1</sup> MnO <sub>2</sub>	1.25:1	2.9:1	1.6:1	n.d.	19		2.5 <sub>initial</sub> 4.5 <sub>end</sub>	1.1 0.7
0.1 molL <sup>-1</sup> MnO <sub>2</sub>	0.73:1	2.0:1	1.2:1	n.a.	21	2	6.2 <sub>initial</sub> 6.0 <sub>end</sub>	0.6 0.5

0.1 molL <sup>-1</sup> MnO <sub>2</sub> + 0.05 molL <sup>-1</sup> CaCO <sub>3</sub>	1.0:1	2.4:1	1.5:1	n.a.	8	2	8.0 <sub>initial</sub> 6.5 <sub>end</sub>	0.6 0.5
0.05 molL <sup>-1</sup> CaCO <sub>3</sub>	1.1:1	3.0:1	1.7:1	n.a.	14	2	9.2 <sub>initial</sub> 6.3 <sub>end</sub>	0.6 0.5

---

893

894

895

896 Table 2 Elemental ratios in chromitite and clinochlore and elemental ratios in the solutions after  
 897 the bulk dissolution experiments with 100 mg chromite powder in 25 mL solution for four  
 898 weeks(with pH value)

Experiment	Cr:Al	Cr:Fe	Cr:Si	pH	
				initial	end
Chromitite	4.5:1	2.1:1	18.7:1		
Clinochlore	1:3	2.2:1	1:14		
Bacteria + TK solution <sup>1</sup>	1:2.5	1:1492	1:3.2	2.1	2.18
TK solution <sup>1</sup>	1:2.5	1:1607	1:3.3	2.1	2.36
Solution A	1:2.8	1:1	1:4.5	2.5	2.35
Bacteria + Solution A	1:2.9	1:17.5	1:4.4	2.1	2.2
H <sub>2</sub> O	2.3:1	2.0:1	1:14.9	7	6.7
TK solution <sup>1</sup> + 0.1 mol L <sup>-1</sup> MnO <sub>2</sub>	1:8.4	1:1461	1:11.5	2.1	2.27
Solution A +0.1 molL <sup>-1</sup> MnO <sub>2</sub>	1.3:1	1:1.6	1:145	2.1	4.28
0.1 molL <sup>-1</sup> MnO <sub>2</sub>	1.4:1	1:1.3	1:135	6.2	6.7
0.1 molL <sup>-1</sup> MnO <sub>2</sub> + 0.05 molL <sup>-1</sup> CaCO <sub>3</sub>	5.6:1	3.7:1	1:18	8.0	7.65
0.05 molL <sup>-1</sup> CaCO <sub>3</sub>	3.0:1	16.3:1	1:12.6	9.2	7.81

899 <sup>1</sup> contain Fe<sup>2+</sup>-sulfates

900

901

902

903

904

905

906 Table 3 Results of the XPS measurement after dissolution experiments with pyrolusite powders

<b>Experiment</b>	pH	Mn [at%] <sup>1</sup> on the surfaces of chromitite	Cr [at%] <sup>1</sup> on the surfaces of MnO <sub>2</sub> particles	Fe [at%] <sup>1</sup> on the surfaces of MnO <sub>2</sub> particles
0.1 molL <sup>-1</sup> MnO <sub>2</sub>	8.0 <sub>initial</sub>	2.0	6.3	3.1
0.05 molL <sup>-1</sup> CaCO <sub>3</sub>	6.5 <sub>end</sub>			
0.1 molL <sup>-1</sup> MnO <sub>2</sub>	6.2 <sub>initial</sub>	22.1	6.4	2.9
	6.0 <sub>end</sub>			
Solution A	2.5 <sub>initial</sub>	3.6	8.3	2.9
0.1 molL <sup>-1</sup> MnO <sub>2</sub>	4.5 <sub>end</sub>			

907 1. percentage relative to all other cations (O and H not included in quantification)

908

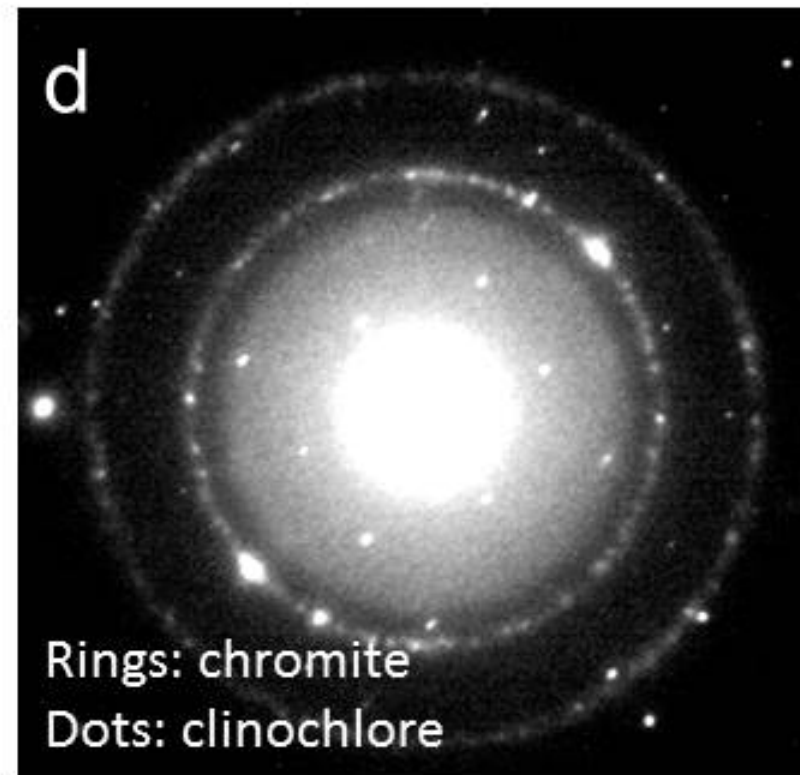
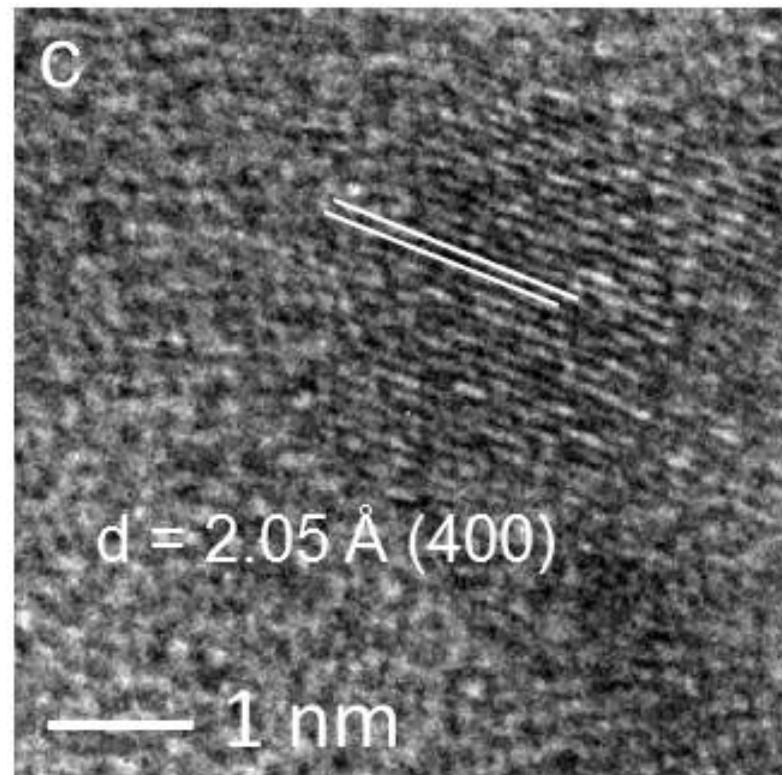
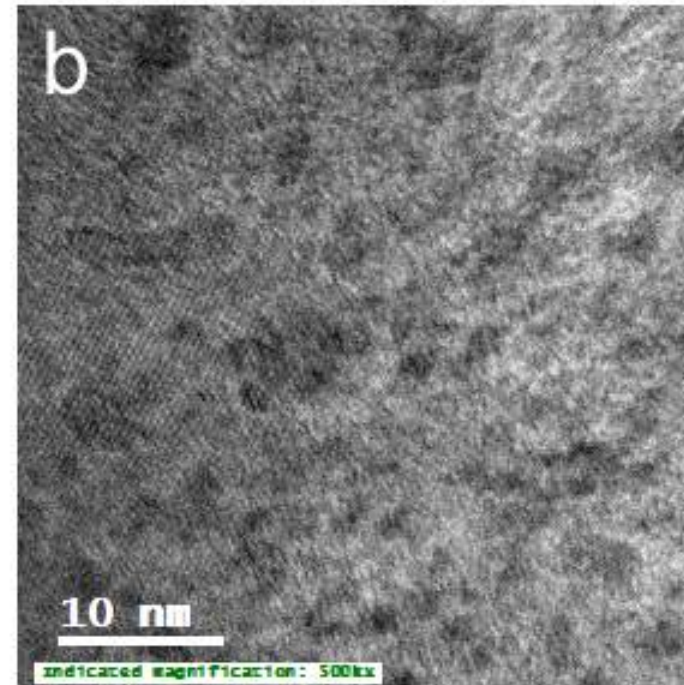
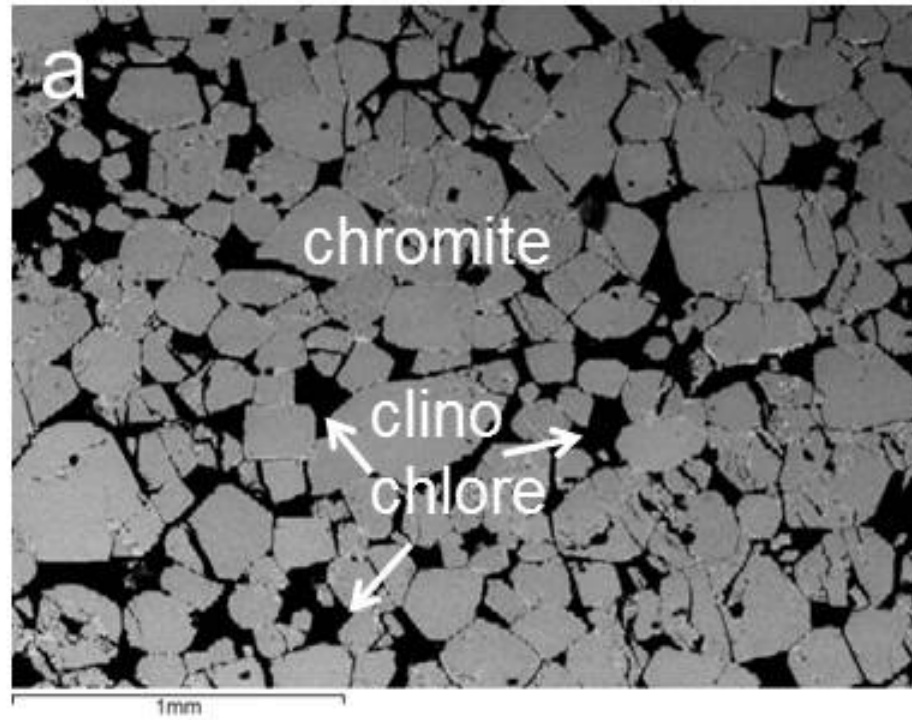


Fig. 1

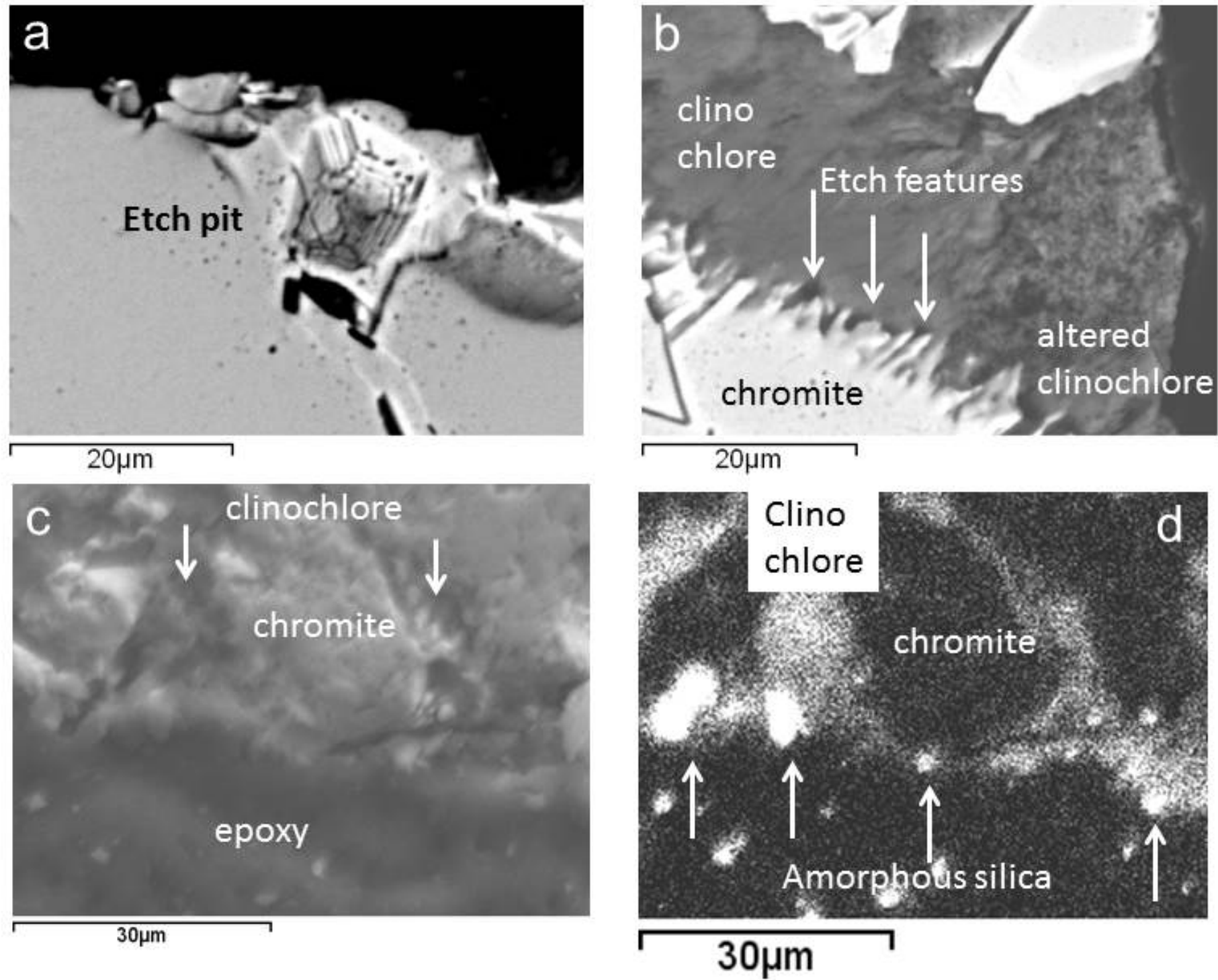


Fig. 2

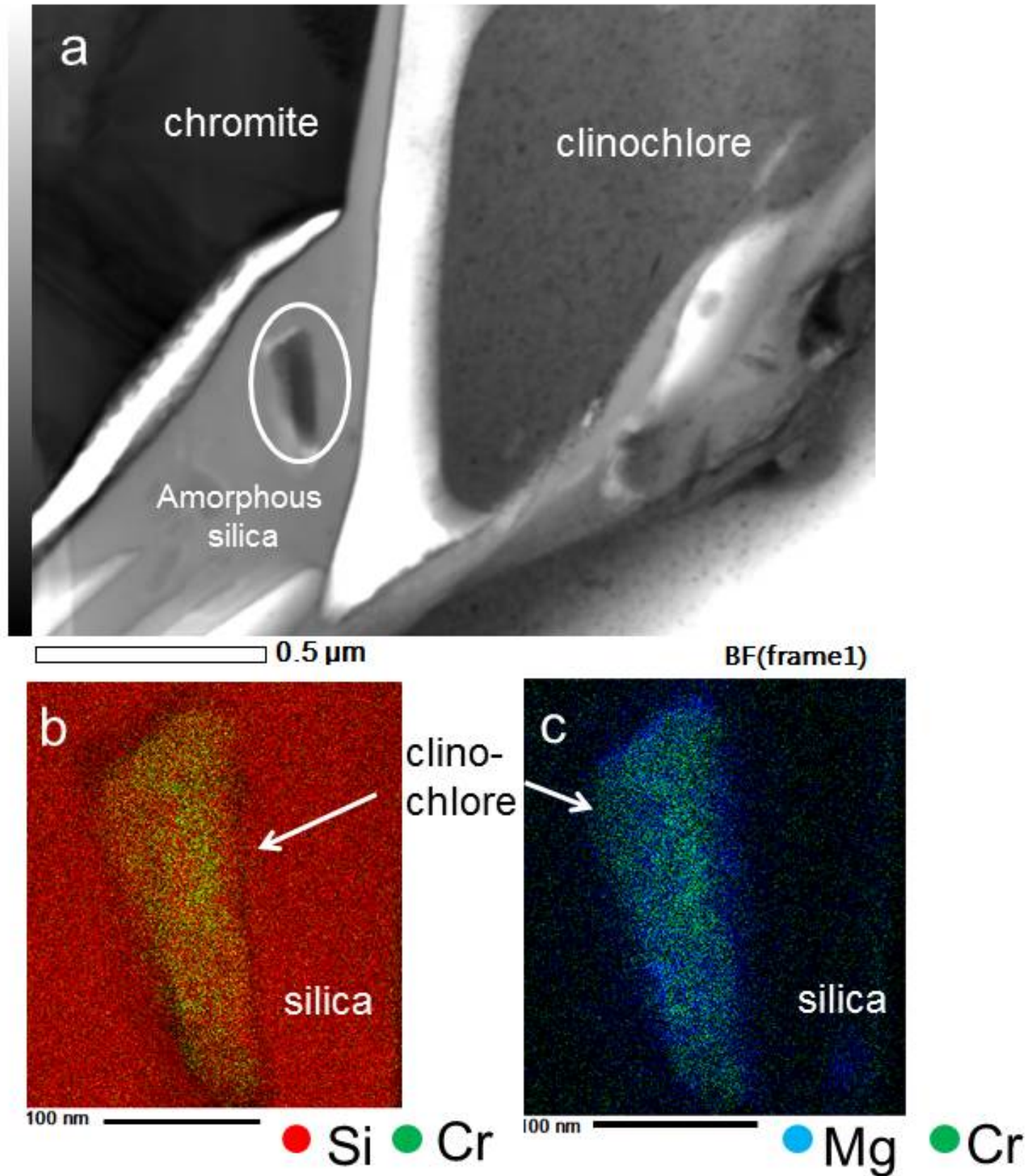


Fig. 3

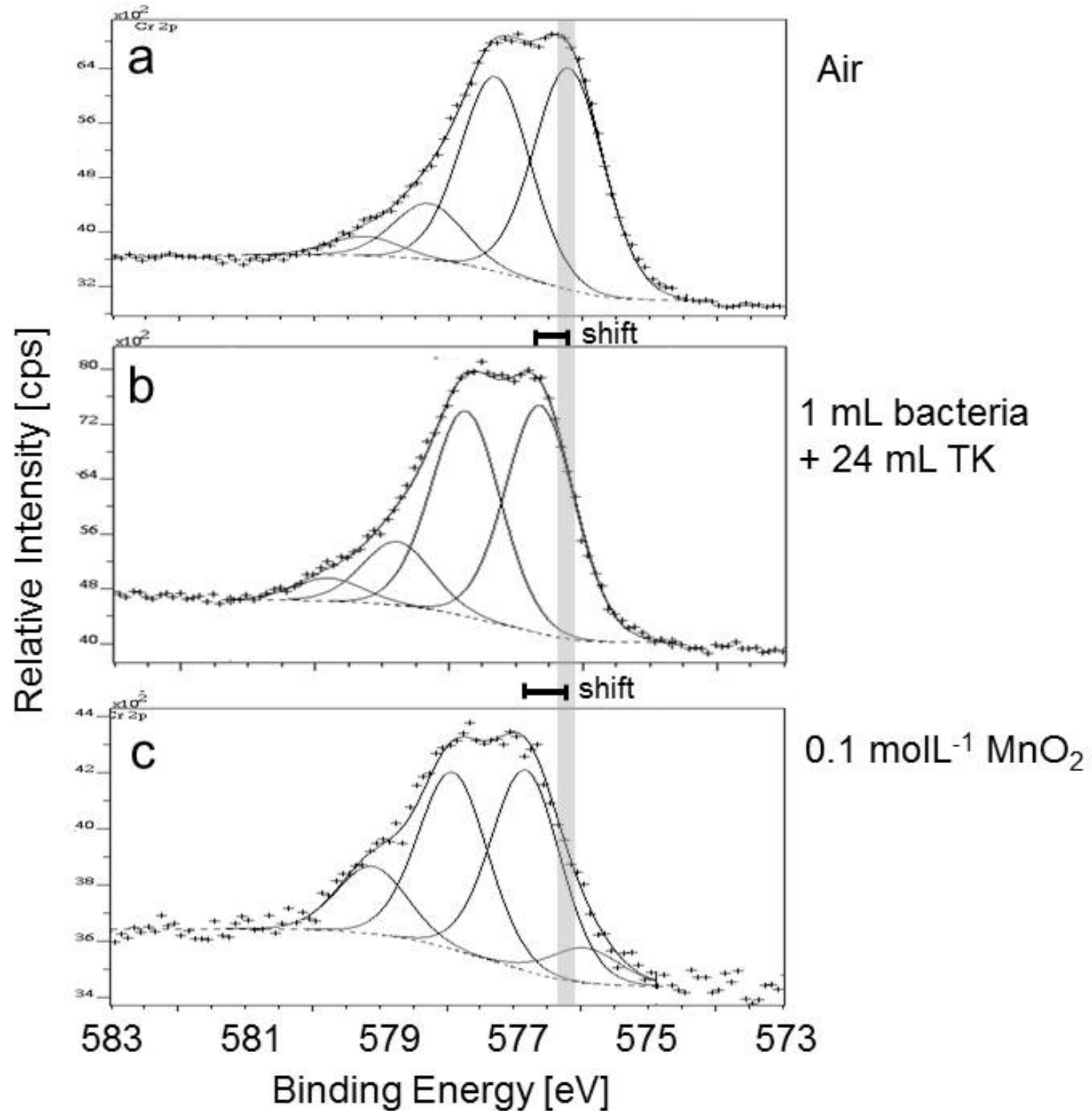


Fig. 4

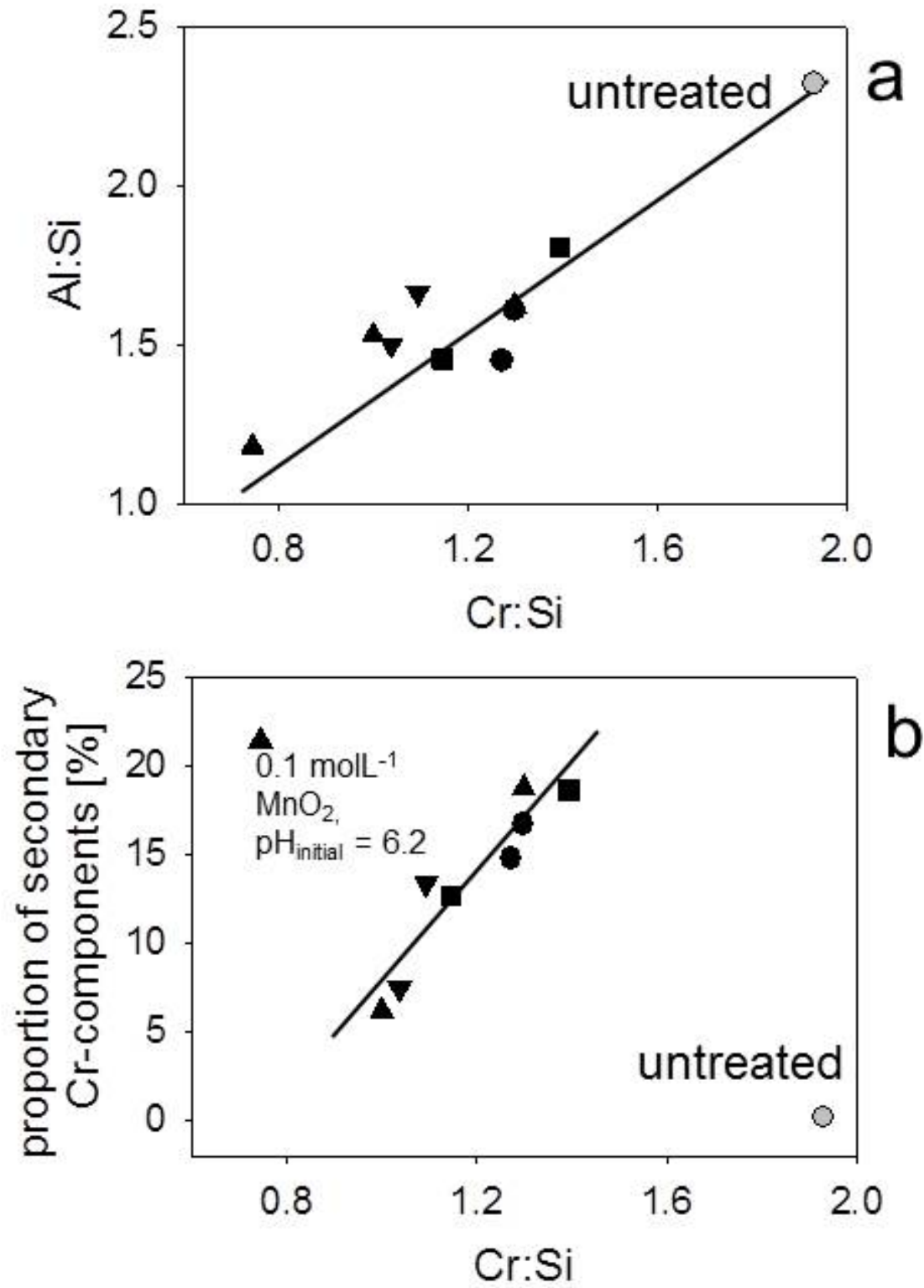


Fig. 5

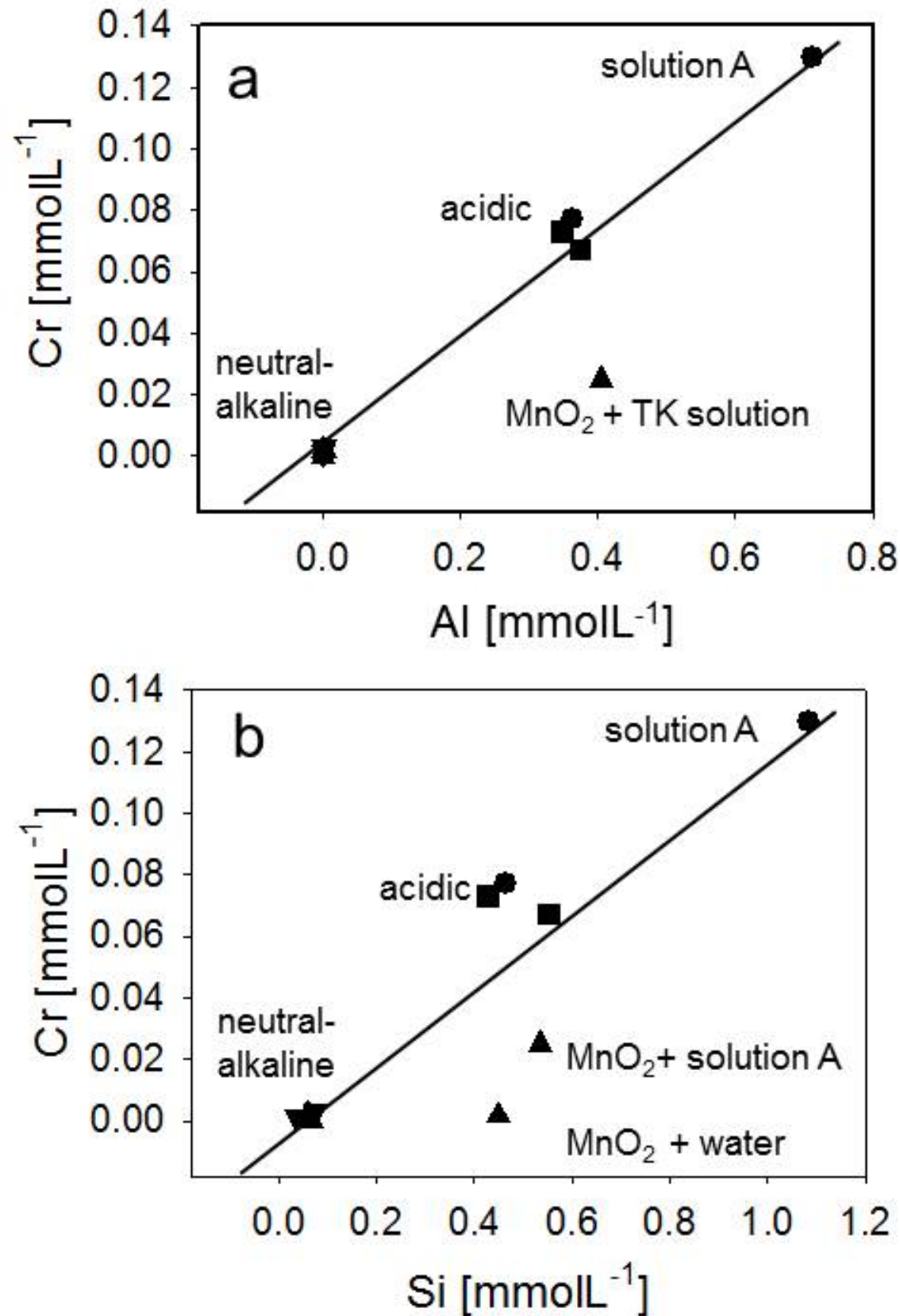


Fig. 6